Revision 1

Unusual replacement of Fe-Ti oxides by rutile during retrogression in amphibolite-hosted veins (Dabie UHP terrane): A mineralogical record of fluid-induced oxidation processes in exhumed UHP slabs

SHUN GUO[1, 2]*, PAN TANG[1,3], BIN SU[1,3], YI CHEN[1, 2], KAI YE[1], LINGMIN ZHANG[4], YIJIE GAO[1,3], JINGBO LIU[1], YUEHENG YANG[1]

[1]State Key Laboratory of Lithospheric Evolution, Institute of Geology and Geophysics, Chinese Academy of Sciences, P.O. Box 9825, Beijing 100029, China

[2]CAS Center for Excellence in Tibetan Plateau Earth Sciences, Beijing 100101, China

[3]University of Chinese Academy of Sciences, Beijing 100049, China

[4]State Key Laboratory of Marine Geology, Tongji University, Shanghai 200092, China

* Corresponding author. Tel.: +86 10 82998515; fax: +86 10 62010846

E-mail address: guoshun@mail.iggcas.ac.cn (S. Guo).

ABSTRACT

The replacement of rutile by Fe-Ti oxides is a common phenomenon during the retrogression of eclogites. Here, we report an unusual case regarding the replacement of Fe-Ti oxides by rutile during greenschist-facies metamorphic overprinting of veins in amphibolites (retrograded eclogites) from the Dabie ultra-high pressure (UHP) terrane, eastern China. The veins mainly consist of plagioclase, Fe-Ti oxides, and quartz and they crystallized from a Ti-rich amphibolite-facies fluid that formed during exhumation of the eclogites. Two types of textures involving the replacement of Fe-Ti oxides by rutile are recognized in the veins: (1) the first type is characterized by the development of rutile coronas (Rt-C) and other silicates (high-Fe epidote, muscovite, and chlorite) around the external boundaries of the Fe-Ti oxide grains, and (2) the second type is characterized by the formation of symplectitic intergrowths of rutile (Rt-S) and magnetite after exsolved hemo-ilmenite (H-Ilm) lamellae in the Fe-Ti oxides. The micro-textures, mineral assemblages, and Zr-in-rutile thermometry indicate that both replacement reactions involved mineral re-equilibration processes in the presence of an infiltrating fluid phase at ~476-515 °C, taking place by an interface-coupled dissolution-precipitation mechanism. Thermodynamic modeling reveals that both replacement reactions occurred during oxidation processes under relatively high oxygen fugacity (fO_2) conditions, approximately 2.5-4.5 logfO_2 units higher than the FMQ (fayalite-magnetite-quartz) reference buffer. In situ Sr isotopic analyses of epidote (Ep-C) coexisting with the Rt-C suggest that the infiltrating fluid involved in the greenschist-facies replacement reactions was externally derived from the surrounding granitic gneisses (the wall rocks of the amphibolites). Compared with the rutile in the UHP eclogites (Rt-E) and amphibolites (Rt-A), the Rt-C is characterized by distinctly lower contents of Nb (<10 ppm) and Ta (<2 ppm) and

Nb/Ta ratios (<10) and higher contents of Cr (>340 ppm) and V (>1580 ppm). These results provide a geochemical fingerprint for distinguishing the low-pressure (LP) rutile from relic high-grade phases in retrograded HP-UHP rocks.

Our results reveal that rutile can form during LP retrograde stage in UHP rocks by high-fO_2 fluid-induced replacement reactions. The unusual replacements of Fe-Ti oxides by rutile-bearing assemblages during retrogression provide important constraints on fluid-mineral reactions and fO_2 variations in exhumed UHP slabs.

Keywords:

Rutile, Fe-Ti oxides, replacement reaction, fluid, oxygen fugacity, exhumation, Dabie UHP terrane

INTRODUCTION

Rutile (TiO_2) is a common accessory mineral in various metamorphic, magmatic, and sedimentary rocks as well as some extraterrestrial samples. Rutile is of particular interest in high-grade metamorphic rocks (e.g., eclogite, granulite, and amphibolite) because it can preserve a wealth of information on the physicochemical conditions during metamorphic growth (Meinhold 2010), which can be used to describe the rock genesis, metamorphic history, and the evolution of orogenic belts. Rutile is a primary host mineral of Nb and Ta and contains minor amounts of Zr, Hf, Cr, V, Fe, Sn, U, and Th. These geochemical characteristics enable rutile to have multiple applications in the solid earth sciences (see review in Meinhold 2010). For example, it can be used to (1) monitor geological processes involving Nb-Ta mobilization and fractionation (e.g., Xiao et al. 2006; Gao et al. 2007; Zhang et al. 2008; Schmidt et al. 2009); (2) obtain the temperature conditions using Zr-in-rutile thermometers (e.g., Zack et al. 2004; Watson et al. 2006; Ferry and Watson 2007; Tomkins et al. 2007); (3) provide age information via U-Pb dating of rutile (e.g., Mezger et al. 1989; Li et al. 2003; Ewing et al. 2015); and (4) trace the origin and evolution of rutile-bearing rocks on the basis of Hf-O isotopic data (e.g., Meinhold et al. 2008; Ewing et al. 2011). In addition, because the growth of rutile often involves the consumption of Fe-Ti oxides (and vice versa), petrological constraints on rutile provide insights into the magnetic properties and anomalies in rocks from subducted slabs and collisional orogens (e.g., Strada et al. 2006). Accurately understanding the growth mechanism and stability field of rutile is important to rigorous geologic applications and reasonable interpretations.

Rutile is generally accepted to mainly occur in high-grade metamorphic rocks and to form under relatively high-pressure (HP) or high-temperature (HT) conditions (Meinhold 2010). Several studies have also found that rutile can occasionally form in

low-grade metamorphic rocks (greenschist and phyllite) (e.g., Luvizotto and Zack 2009; Luvizotto et al. 2009). Most present models favor the interpretation that metamorphic rutile forms from the replacement of pre-existing Ti-rich phases, such as high-Ti biotite, titanite, and Fe-Ti oxides during prograde to peak metamorphic stages (e.g., Zack et al. 2002; John et al. 2011; Luvizotto and Zack 2009; Luvizotto et al. 2009). In contrast, during retrogression, rutile partially or totally transforms into the Ti-rich phases listed above in association with decreases in temperatures and/or pressures. The direct mineralogical record of the latter process is the formation of Fe-Ti oxides and/or titanite rims around rutile in retrograded eclogites, amphibolites, and other lithologies (e.g., Yang 2004; Lucassen et al. 2010; Cruz-Uribe et al. 2014).

In addition to *P-T* conditions, the redox state is another potential factor that could influence the stability ranges of rutile and Fe-Ti oxides (e.g., Lindsley 1991; Braun and Raith 1985; Rečnik et al. 2015; Tan et al. 2015). High oxygen fugacity (fO_2) conditions generally facilitate the oxidation of ferrous to ferric iron in Fe-Ti oxides, thereby promoting the removal of iron from Fe-Ti phases and consequently triggering crystallization or exsolution of rutile. This process is known from the formation of secondary rutile or intermediates (e.g., pseudorutile and ferropseudobrookite) by the oxidation of primary ilmenite in dykes, intrusions, and paleoplacers during hydrothermal alteration and chemical weathering (e.g., Temple 1966; Sakoma and Martin 2002; Hébert and Gauthier 2007). More recently, Tan et al. (2015) and Rečnik et al. (2015) noted unique intergrowths of rutile + magnetite and rutile + hematite, respectively, formed from single- or multiple-stage oxidation of ilmenite-hematite solid solutions (Ilm-Hem_{ss}). In a metamorphic system, Braun and Raith (1985) found that hemo-ilmenite (H-Ilm) and ilmeno-hematite (I-Hem) in metabasites from the eastern Alps of Austria developed into rutile-bearing assemblages under oxidizing

conditions during low grade metamorphism. Metamorphic fluid/melt infiltration, accompanied by different degrees of fluid-rock interaction, is a key factor responsible for variations in the redox state of metasomatized rocks (Connolly and Cesare 1993; Mattinson et al. 2004; Rowe et al. 2009; Guo et al. 2014). This fact demonstrates that, in zones with high fluid fluxes, such as bleach zones or vein systems, the stabilities of rutile and Fe-Ti oxides are more susceptible to being affected by the f_{O_2} conditions. Redox state should be carefully considered when interpreting the growth mechanisms and stability conditions of rutile that crystallized in these geologic environments.

In this study, we report a rare case of retrograde rutile growth during cooling by the replacements of Fe-Ti oxides in veins hosted by amphibolites [retrograde ultra-HP (UHP) eclogite] from the Dabie terrane, China. We investigate the occurrence, texture, and geochemistry of the low-pressure (LP) rutile and reveal that the formation of the LP rutile at the expense of Fe-Ti oxides was caused by the infiltration of an externally derived high-f_{O_2} fluid during greenschist-facies metamorphism. Our results highlight that the occurrence of LP rutile replacing Fe-Ti oxides bears important implications for fluid-mineral reactions and physicochemical condition variations in exhumed UHP slabs.

GEOLOGICAL SETTING

The Dabie-Sulu UHP metamorphic terrane in east-central China was formed by northward subduction and collision of the South China Block beneath the North China Block in the Triassic (Zhang et al. 2009). The Dabie terrane makes up the western segment of the Dabie-Sulu UHP terrane, which is separated by approximately 500 km of left-lateral strike-slip displacement along the Tan-Lu fault (Appendix Fig. A1a). The UHP rocks in the Dabie terrane mainly consist of various types of gneisses, with small quantities of eclogite, garnet peridotite, pyroxenite, marble, and jadeite quartzite.

The extensive occurrence of coesite in various lithologies indicates that the majority of the Dabie terrane has experienced UHP metamorphism (e.g., Liu and Liou 2011). Most of the gneisses and eclogites have Neoproterozoic protolith ages ranging from 740 to 800 Ma (e.g., Zheng et al. 2006; Liu and Liou 2011). High-resolution U-Pb dating of zircon or monazite from various rock types indicates four discrete and meaningful metamorphic ages for the Dabie terrane (e.g., Ayers et al. 2002; Liu et al. 2008; Liu and Liou 2011): (1) 246-244 Ma for prograde eclogite-facies metamorphism; (2) 235-225 Ma for UHP metamorphism; 225-210 Ma for HP recrystallization; and (4) 215-205 Ma for amphibolite-facies retrogression. In addition, Rb-Sr and Sm-Nd isotopic chronologies indicate that UHP rocks experienced a slow cooling process (from 500 to 450 °C, corresponding to greenschist-facies conditions) from ~219 to 180 Ma (Li et al. 2000).

The present study area is located east of the Hualiangting Reservoir (NW of the county of Taihu) in the Dabie UHP terrane (Appendix Fig. A1b), where mafic UHP eclogites and amphibolites occur as blocks or small lenses within muscovite-rich magnetite-bearing orthogneiss (Guo et al. 2015, 2016). The studied outcrop is an approximately 400-m-long massive mafic block of eclogites and amphibolites. The fresh or weakly retrograded UHP eclogites are locally preserved in the interior of the mafic block and are characterized by the development of hydrous porphyroblasts (epidote and amphibole) (Massonne 2012; Guo et al. 2015, 2016) and prismatic mineral assemblages after lawsonite (Guo et al. 2015). Epidote-rich amphibolites (Fig. 1a), which are the retrograde equivalents of UHP eclogite, constitute approximately 70 percent of the volume of the metabasite block. Rolfo et al. (2000) suggested that the Hualiangting eclogite experienced a clockwise *P-T* path with metamorphic peak conditions of ≥2.6-2.7 GPa and 710 ± 20 °C. Shi and Wang (2006) estimated that the

peak *P-T* conditions of the eclogites ranged from 2.0 to 3.5 GPa and 640 to 840 °C. Massonne (2012) argued that the eclogites originated from a granulite precursor and experienced a counterclockwise *P-T* path with peak conditions of >3.5 GPa and >800 °C. Guo et al. (2015) proposed a clockwise *P-T* path for the UHP eclogites. Their results indicated significant fluid liberation induced by the breakdown of lawsonite in the eclogites during the initial exhumation stage (~2.8-3.0 GPa and 660-720 °C). The amphibolite-facies retrogression of the Hualiangting eclogites was estimated to have occurred at 0.8-1.0 GPa and 646-674 °C (Guo et al. 2016).

Abundant low-pressure (LP) leucocratic plagioclase-rich veins are found in the amphibolites (Figs. 1a and 1b). These veins generally occur as vimineous, isolated, and irregularly shaped fractures in the host amphibolites and exhibit sharp margins with the amphibolites. The LP veins are typically on the order of 2-15 cm in width and 0.5-8 m in length and crosscut the dominant foliation at intermediate to high angles (Figs. 1a and 1b). No obvious alteration haloes around the LP veins are observed. The LP veins develop various amounts of coarse-grained (up to centimeter scale), tabular or prismatic, dark-colored Fe-Ti oxides, which are mainly distributed in the interior of the veins (Fig. 1b).

SAMPLE DESCRIPTION

The investigated samples in this study include two UHP eclogites (09HLT20 and 09HLT21), two amphibolites (09HLT23A and 09HLT24A), and two plagioclase-rich veins (09HLT23V and 09HLT24V). The mineral assemblages and mineral volume abundances of these samples are listed in Appendix Table 1. The whole-rock and mineral compositions and epidote Sr isotopes of these samples were analyzed. The analytical methods and procedures are presented in Appendix text.

The eclogites are composed of garnet (45 vol%), omphacite (30-34 vol%), and

epidote (8-12 vol%) with minor amounts of quartz, kyanite, barroisite, rutile and zircon (Fig. 2a). The amphibolites are composed of amphibole (45 vol%), plagioclase (26-28 vol%), epidote (15-17 vol%), and quartz (8 vol%) with minor amounts of Fe-Ti oxides, rutile, and apatite (Figs. 2b-2e). Both the eclogites and amphibolites have basaltic compositions with TiO_2 contents of 1.8-2.2 wt%, Na_2O contents of 2.5-3.6 wt%, and K_2O contents of 0.2-0.5 wt% (Appendix Table 2) and exhibit light rare earth element (LREE)-rich patterns (Appendix Fig. A2a). The large ion lithophile element (LILE: Cs, Rb, Ba, and Sr) contents of the eclogites and amphibolites are relatively low (5-50 times primitive mantle values, Appendix Fig. A2b). The Nb/Ta ratios of the eclogites (17-20) are similar to those of the amphibolites (20-21).

The veins are primarily composed of plagioclase (80-88 vol%), Fe-Ti oxides (5-12 vol%), and quartz (5 vol%) (Figs. 1b and 3a-3d). Minor apatite, rutile, epidote, muscovite, chlorite, and zircon are also observed in the veins (Figs. 1c-1e and 3e-3h). The veins have higher SiO_2, Al_2O_3, and Na_2O contents and lower CaO content than the host metabasites (Appendix Table 2). The FeO (0.3-1.7 wt%), Fe_2O_3 (1.4-9.5 wt%) and TiO_2 (0.4-2.7 wt%) contents vary among the samples, depending on the abundance of the Fe-Ti oxides. The veins have overall lower rare earth element (REE), U, and Th contents than the metabasites and display a LREE-depleted and heavy REE (HREE)-flat pattern (Appendix Fig. A2a). The LILE contents of the veins are similar to those of the metabasites, while the HFSE (Nb, Ta, Zr, Hf) contents of the veins are lower than those of the metabasites (Appendix Fig. A2b). The veins have lower Nb/Ta ratios (11-14) than the metabasites.

MICROTEXTURES INVOLVING RUTILE AND FE-TI OXIDES

The major Ti-rich phases in the metabasites and veins are rutile and Fe-Ti oxides. The rutile in different lithologies was confirmed by its Raman bands at *ca.* 142-143,

241-242, 445-447, and 612 cm^{-1} (peak positions) (Appendix Fig. A3), which rule out the possibility that these phases are other TiO_2 polymorphs (anatase or brookite).

Eclogites and amphibolites

Rutile in the eclogites (Rt-E) occurs as rounded, anhedral grains ranging from 30 to 400 μm in size (Table 1; Fig. 2a). The Rt-E is in textural equilibrium with garnet, omphacite, and epidote (Ep-E) or occurs as inclusions in these minerals. The coexistence with coesite implies that the Rt-E formed during the UHP stage (Guo et al. 2015). The Rt-E has experienced very weak retrograde overprinting, and most of the Rt-E grains are not rimmed by Fe-Ti oxide or titanite coronas. No exsolution lamellae are found in the Rt-E.

Rutile in the amphibolites (Rt-A) is very rare, and it usually occurs as relic cores (10-80 μm in size) surrounded by corona rims of polycrystalline Fe-Ti oxides (20-200 μm in size) (Figs. 2b and 2c). In addition to rims around the Rt-A, anhedral Fe-Ti oxides also occur as independent phases in the silicate matrix (Figs. 2b and 2d). The Fe-Ti oxides are in textural equilibrium with amphibole, plagioclase, and epidote (Ep-A) or contain inclusions of these minerals (Figs. 2b-2e). High-contrast BSE images show that a single Fe-Ti oxide grain is composed of I-Hem that exsolved a set of well-oriented H-Ilm lamellae (Figs. 2e and 2f). The H-Ilm lamellae can be divided into two groups based on their widths: the coarse lamellae have widths of 4-8 μm while the thin lamellae have widths of <1 μm. The volume ratio (assumed to be equal to area ratio) of the exsolved H-Ilm lamellae to the I-Hem matrix is estimated to be approximately 1:3, according to the statistics on multiple Fe-Ti oxide grains (Fig. 2f).

Plagioclase veins

Fe-Ti oxides are a major constituent of the plagioclase veins. Similar to those in the amphibolites, each Fe-Ti oxide mineral in the veins is also composed of an I-Hem

matrix and two groups (coarse and fine) of well-oriented H-Ilm lamellae (Figs. 3c and 3d). The coarse spindle-shaped lamellae range from 2 to 10 μm in width and from 10 to 40 μm in length, while the fine needle-like lamellae have widths of <1 μm and lengths of 1-40 μm. The volume ratio (assumed to be equal to area ratio) of the H-Ilm lamellae to the I-Hem matrix in Fe-Ti oxide grains is approximately 1:3 (Fig. 3d).

Rutile in the veins occurs in two distinct microstructural settings (Table 1). The first type of rutile appears as small, rounded to flat, polycrystalline grains around the external edges of the Fe-Ti oxides and forms continuous or discontinuous coronas (Rt-C) that are 30-150 μm thick (Figs. 1c-1d, 3a, and 3b). Locally, a thin continuous cover of small Rt-C grains, up to 5 mm in length, is observed on the Fe-Ti oxides (Fig. 1c). The boundaries between the Fe-Ti oxides and Rt-C are either a zigzag shape, generated by the penetration of fine Rt-C needles into the Fe-Ti oxides (Figs. 3a and 3b) or a relatively smooth curve (Fig. 3e). The original shapes of Fe-Ti oxide grains are preserved, and the reaction interface moving through the parent grain can be observed. Micro-fractures with various extensional orientations are present throughout entire Fe-Ti oxide-rutile grains (Fig. 3a). The Rt-C typically coexists with fragmental, porous, polycrystalline epidote (Ep-C) and muscovite (Figs. 3f-3h) and occasionally coexists with anhedral polycrystalline chlorite (Fig. 3f). Minor amounts of Rt-C are found as inclusions in Ep-C (Fig. 3g) and chlorite, indicating the synchronous growth of Rt-C, Ep-C, and chlorite. The Rt-C is also found to coexist with quartz and zircon.

The other type of rutile in the veins is always associated with the exsolved coarse H-Ilm lamellae in the interior of Fe-Ti oxides. Intergrowths of fine-grained (1-5 μm) vermicular rutile (Rt-S) and interstitial magnetite occur as symplectites after H-Ilm lamellae (Fig. 4). The intergrowths generally develop in the H-Ilm lamellae that are spatially close to fine fractures (Fig. 4a) extending to the outside of the Fe-Ti oxide

grains. In contrast, in the regions where fractures are absent, the primary textures and compositions of H-Ilm lamellae remain unchanged. The symplectites almost preserve the size and morphology of the former H-Ilm lamellae, indicating a pseudomorphic replacement process (Figs. 4b and 4c). Relics of H-Ilm occasionally occur within the symplectites (Figs. 4b-4e). Variously sized intergranular voids or cavities are observed in the symplectite interiors or along the boundaries between the symplectites and Fe-Ti oxides (Figs. 4b-4e). The symplectites of Rt-S + magnetite mainly occur in the Fe-Ti oxide grains that developed Rt-C.

MINERAL GEOCHEMISTRY

Rutile

The different types of rutile show a large variation in trace element compositions (Table 2; Fig. 5). The Rt-E has high Nb (140-220 ppm), Ta (8-12 ppm), Zr (79-108 ppm), Cr (110-260 ppm), and V (1050-2080 ppm) contents (Figs. 5a-5c) and Nb/Ta ratios (13-24, Fig. 5d). There is a limited intra-grain compositional variation for the Rt-E. The Rt-A has higher Nb (190-540 ppm), Ta (9-22 ppm), and Zr (117-175 ppm) contents and Nb/Ta ratios (16-25) than the Rt-E. The Cr and V contents of the Rt-A are similar to or slightly lower than those of the Rt-E. Because the grain sizes of most of the Rt-A are very small (generally <80 μm, Figs. 2b and 2c), the compositional variation along a traverse in a single Rt-A grain was not examined. However, analyses on multiple Rt-A grains indicate that the Rt-A has a broader range of Nb content than the Rt-E (Figs. 5a and 5c).

The Rt-C has noticeably lower Nb (0.5-10 ppm), Ta (0.1-1.8 ppm), and Zr (15-30 ppm) contents (Figs. 5a-5c) and Nb/Ta ratios (2-10) (Fig. 5d) than the Rt-E and Rt-A. The Cr (340-790 ppm) and V (1580-3010 ppm) contents of the Rt-C are higher than those of the Rt-E and Rt-A (Figs. 5a and 5c). The trace element compositions of the

rutile coronas in the amphibolites (Fig. 2c) and the Rt-S in the veins (Fig. 4) were not analyzed due to the small grain sizes.

Fe-Ti oxides (H-Ilm, I-Hem, and magnetite)

The coarse H-Ilm lamellae in the Fe-Ti oxides from the amphibolites and veins have similar compositions, with 52-54 wt% FeO and 44-46 wt% TiO_2 (Appendix Table 3). The H-Ilm is composed of 84-88 mol% ilmenite and 12-16 mol% hematite (or 82-87 wt% ilmenite and 12-17 wt% hematite) (Appendix Table 3; Appendix Fig. A4).

The compositions of the I-Hem matrix in the Fe-Ti oxides from the amphibolites and veins are similar. The I-Hem is composed of 72-76 mol% hematite and 24-28 mol% ilmenite (or 73-76 wt% hematite and 23-27 wt% ilmenite) (Appendix Table 3; Appendix Fig. A4).

The bulk compositions of the Fe-Ti oxides (i.e., Ilm-Hem_{ss} precursors) were calculated in terms of the measured compositions of the H-Ilm lamellae and I-Hem matrix and the relative volume percents of the H-Ilm (25 vol%) and I-Hem (75 vol%). The results show that the Ilm-Hem_{ss} precursors in the amphibolites and veins have similar average compositions: ~72 wt% FeO (total iron) and ~21 wt% TiO_2 (Appendix Table 3). The trace element analyses reveal that the Ilm-Hem_{ss} precursors in both amphibolites and veins have low Nb (0.4-4.7 ppm), Ta (0.1-1.6 ppm), Zr (2.8-21.5 ppm), and Hf (0.2-2.3 ppm) contents and high Cr (490-980 ppm) and V (2460-6350 ppm) contents. The Nb/Ta ratios of the Ilm-Hem_{ss} precursors range from 2 to 10. Both trace element contents and element ratios of the Ilm-Hem_{ss} precursors are close to those of the Rt-C (Appendix Table 4; Fig. 5).

The magnetite in the symplectites contains ~0.6-3 wt% TiO_2 and is composed of ~91-98 mol% magnetite and 1-9 mol% ulvöspinel (or 92-98 wt% magnetite and ~2-8

wt% ulvöspinel) (Appendix Table 3). The trace element compositions of magnetite were not analyzed due to the small grain sizes.

Epidote

The Ep-E and Ep-A in the metabasites have low X_{Fe} [$=Fe^{3+}/(Fe^{3+}+Al)$, all Fe is assumed to be Fe^{3+}] values of 0.23-0.26 (Appendix Table 5; Fig. 6). The Ep-C in the veins has noticeably higher X_{Fe} values (0.32-0.38) than the Ep-E and Ep-A (Fig. 6).

The compositions of other minerals (muscovite, chlorite, amphibole, plagioclase, and apatite) were presented in Appendix Table 6 and described in the Appendix text.

ZR-IN-RUTILE THERMOMETRY

The partitioning of Zr into rutile coexisting with zircon and a SiO_2 polymorph has been proven to be temperature dependent. In this study, the formation temperatures of Rt-E in the eclogites and Rt-C in the veins are calculated in terms of the measured Zr contents in the rutile (Table 2; Figs. 7a and 7b) using the Zr-in-rutile thermometer of Tomkins et al. (2007), whose model includes a pressure correction term. Due to widespread occurrence of zircon and quartz in the matrix of the eclogites, Rt-E are considered to be in equilibrium with zircon and quartz (or coesite), as suggested by many previous studies (e.g., Zack et al. 2002; Zheng et al. 2011). Zircon and quartz grains are also observed to coexist with vein Rt-C (Fig. 7b). As a consequence, Zr-in-rutile thermometry can be applied under the assumption that $a_{ZrSiO4} = 1$ and $a_{SiO2} = 1$ during the growth of Rt-C.

Different pressure conditions were used for the temperature calculations of the Rt-E and Rt-C (Table 1). Pressure used for the Rt-E is assumed to be 3.5 GPa, based on previous estimates of the peak metamorphism of the Hualiangting eclogites (Massonne 2012; Guo et al. 2015). The Zr contents in the Rt-E range from 79 to 108 ppm, yielding temperatures of 636-659 °C (Fig. 7a). This temperature range is in

accordance with that (620-680 °C) estimated via phase equilibrium modeling by Guo et al. (2015).

The growth of the Rt-C occurred later than the amphibolite-facies metamorphic veining (crystallization of Fe-Ti oxides, 0.8-1.0 GPa). The coexistence of chlorite with vein Rt-C indicates that this type of rutile formed during the greenschist-facies retrograde metamorphism. Thus, we use an average pressure for greenschist-facies conditions (0.5 GPa, Spear 1993) to calculate the temperatures of vein Rt-C. The Zr contents in vein Rt-C range from 14 to 30 ppm, yielding temperatures of 476-515 °C (Fig. 7b). Reduction of assumed pressure to 0.4 GPa or increase of the pressure to 0.6 GPa results in an approximately 2 °C variation in calculated temperatures.

IN SITU SR ISOTOPE

In situ Sr isotopic analyses of epidote can provide constraints on the fluid origin in HP-UHP rocks (Guo et al. 2014, 2016). In this study, three types of epidote (Ep-E, Ep-A, and Ep-C) were analyzed (Appendix Table 5). The $^{87}Rb/^{86}Sr$ ratios of all types of epidote are less than 0.001, indicating that the interference of ^{87}Rb on ^{87}Sr is negligible. The initial Sr isotopic ratios of Ep-E, Ep-A, and Ep-C are calculated at the ages of UHP metamorphism (t = 230 Ma), amphibolite-facies metamorphism (t = 210 Ma), and greenschist-facies metamorphism (t = 200 Ma), respectively, for the Dabie eclogites (Li et al. 2000; Liu and Liou 2011).

Analyses of twelve points on the Ep-E yield a limited variation in the initial $^{87}Sr/^{86}Sr$ ratios, ranging from 0.70433 to 0.70454. Analyses of twelve points on the Ep-A yield an essentially similar initial $^{87}Sr/^{86}Sr$ ratio range (0.70439 to 0.70457) as the Ep-E. However, analyses of fourteen points on the Ep-C yields a larger range of the initial $^{87}Sr/^{86}Sr$ ratios, ranging from 0.70511 to 0.70701 (Fig. 6).

The initial $^{87}Sr/^{86}Sr$ ratios of the Ep-E and Ep-A are identical to those of the

eclogites and amphibolites (Guo et al. 2015, 2016) within analytical uncertainty. The initial $^{87}Sr/^{86}Sr$ ratios of the Ep-C vary between those (t = 200 Ma) of the metabasites (0.7043-0.7048, Guo et al. 2015, 2016) and the wall-rock gneisses (0.7098-0.7108, Guo et al. 2015) (Fig. 6).

DISCUSSION

Formation of Ti-rich plagioclase veins in the amphibolites

Veins are the most intuitive sign of channelized fluid flow in rocks. While eclogite-facies veins (e.g., omphacite-, garnet-, or phengite-bearing veins) in HP-UHP metabasites generally form from aqueous fluids released during prograde or peak metamorphic stages (e.g. Hermann et al. 2006; Spandler et al. 2011; Guo et al. 2012; Klemd 2013), plagioclase-rich veins dominantly occur in retrograded HP-UHP rocks and record fluid migrations during amphibolite- to greenschist-facies retrogression in response to slab exhumation (e.g., Miller et al. 2002; Miller and Cartwright 2006).

The Hualiangting plagioclase veins occur exclusively in the amphibolites and are absent in the eclogites. The occurrences and mineral assemblages of the veins indicate that they crystallized during amphibolite-facies retrograde metamorphism (~646-674 °C and 0.8-1.0 GPa, Guo et al. 2016). The absence of plagioclase veins in the wall rocks (i.e., granitic gneiss) of the metabasites indicates that the vein-forming fluid was internally derived from the metabasite itself rather than from the wall rocks. This interpretation is also in accordance with the fact that the compositional characteristics of the veins (high Na_2O and TiO_2 contents and low K, Cs, and Rb contents, Appendix Fig. A2) are significantly different from those of the fluids/melts released by granitic gneisses (e.g., Xiao et al. 2011). In addition, the veins have much lower REE, U, and Th contents than the metabasites and show a LREE-depleted pattern, suggesting that these veins crystallized from an aqueous fluid rather than a

melt. The vein-forming fluid most likely formed from the breakdown of hydrous minerals (e.g., lawsonite and epidote) in the metabasites during exhumation (e.g., Guo et al. 2013, 2015, 2016). Exsolution of hydroxyl and molecular water from nominally anhydrous minerals in the metabasites might also have contributed to the channelized fluid flows in these rocks (Chen et al. 2007).

The grain size and morphology of the Fe-Ti oxides in the veins are different from those of the Fe-Ti oxides in the host amphibolites (Fig. 1c), indicating that the Fe-Ti oxides in the veins were directly crystallized from the LP vein-forming fluids rather than being mechanically transported from the host rocks via the fluid flow. Therefore, the high abundance of Fe-Ti oxides in the veins indicates high solubilities of Ti and Fe in the fluid. Although titanium has long been considered to be fluid immobile, recent experimental studies have indicated that adding components such as Na, Al, and F can significantly elevate the Ti solubility in the fluid by complexing with Ti to form Na-Ti, Na-Al-Ti, and Ti-F polymers (e.g., Antignano and Manning 2008; Manning et al. 2008; Rapp et al. 2010; Tanis et al. 2016). The Hualiangting veins are dominantly composed of oligoclase (80-86 vol%), which indicates high amounts of Na and Al in solution. F-rich vein apatite (Appendix Fig. A6) implies elevated F contents in the fluids. Therefore, Na-Al-Si-F polymers enhanced the Ti solubilities in the solutions. Once the precipitation of the plagioclase and apatite occurred, the vein-forming fluid became depleted in Na, Al, Si, and F, consequently reducing the solubility of Ti (and other HFSEs) and causing Ti saturation and Fe-Ti phase crystallization. Our results indicate that if the appropriate physicochemical parameters are satisfied, amphibolite-facies fluid can appreciably mobilize and transfer HFSEs.

The exsolution textures (Fig. 3c) in the Fe-Ti oxides from the veins (as well as from the amphibolites) indicate that the originally crystallized Fe-Ti phases were

homogeneous Ilm-Hem_{ss}, which subsequently formed the exsolved H-Ilm lamellae in the I-Hem matrix when the temperature decreased to that of the miscibility gap during cooling (e.g., Lindsley 1973, 1991). Similar exsolution lamellae of H-Ilm or I-Hem in Fe-Ti oxides have been observed in other high-grade metabasites (Braun and Raith 1985; Bingen et al. 2001; Austrheim et al. 2008). Based on the solvus of Ilm-Hem_{ss} established by Braun and Raith (1985), we roughly estimated that the exsolution in the Fe-Ti oxides from both the veins and amphibolites occurred at ~520-530 °C, in terms of the measured compositions of H-Ilm and I-Hem (Appendix Table 3).

Replacement of Fe-Ti oxide minerals by rutile during retrogression in veins

Formation of Rt-C

The corona textures of Rt-C around Fe-Ti oxide grains (Figs. 1c-1e) and the jagged grain boundaries between the two phases (Figs. 3a, 3b, 3g, and 3h) indicate the formation of Rt-C by partial replacement of Fe-Ti oxides. The Rt-C coronas between oligoclase and Fe-Ti oxides typically coexist with Fe^{3+}-rich epidote, muscovite, and chlorite, indicating that this replacement reaction is closely related to fluid-induced metasomatism rather than a pure solid-state reaction or volume diffusion (Putnis 2009; Putnis and Austrheim 2010; Harlov et al. 2011). This is because Ca, Al, and Si in the reaction products can be locally derived from the oligoclase, but H_2O and K must be externally provided by an infiltrating fluid phase. This interpretation is strengthened by the fact that the product Rt-C do not form on all the Fe-Ti oxide boundaries (Fig. 1c), implying that the formation of the Rt-C is only on the sites where fractures have propagated and where infiltrating fluid was able to pass (Putnis and Austrheim 2010). Similar corona textures involving the replacement of Fe-Ti phases by zircon have been observed in metagabbros and granulites from southern and western Norway (Bingen et al. 2001; Austrheim et al. 2008). An interface-coupled

dissolution-precipitation mechanism is generally invoked to account for the formation of such coronas (Putnis and Austrheim 2010 and references therein). In this scenario, fluids are expected to infiltrate into the veins along the grain boundaries between the Fe-Ti oxides and oligoclase, dissolving both phases and producing an interfacial fluid supersaturated with respect to rutile (Ti), epidote (Si, Ca, Al, and Fe), muscovite (Si, K, and Al) and chlorite (Si, Al, Fe, and Mg). The replacement sustainability and reaction front propagation depend on whether available pathways for fluid and mass transfer are maintained (Putnis and Austrheim 2010). The generation of porosity in products, which is controlled by the volume changes and the relative solubilities of the solid minerals, would allow the fluid to maintain contact with the reaction front (Janssen et al. 2010; Putnis and John 2010). In this regard, the thickness of Rt-C reflects the degree of metasomatism and the ability of the infiltrating fluid to access the reaction interfaces.

The most key mass transfer of this replacement is the removal of Fe from former site in Fe-Ti oxide grains and the nucleation of Rt-C. This process involved multiple mineral phases. Based on the petrographic observations, the reactants might contain Fe-Ti oxides (H-Ilm and I-Hem), plagioclase, quartz, and H_2O (fluid) and the products involve Rt-C, Ep-C, muscovite, and chlorite. In addition, the presence of muscovite in the products indicates the involvement of K, which might be provided by the fluid. Based on the mineral assemblages and compositions of the reactants and products (Appendix Tables 3, 5, and 6), we calculated the reactions involving this replacement process using the THERMOCALC program (Powell et al. 1998; version 3.33) and the thermodynamic database of Holland and Powell (2011). Activities of plagioclase, ilmenite, hematite, epidote, and chlorite were calculated from measured compositions by the AX program of Holland and Powell (1998). Quartz, water, and rutile were

treated as pure end-member phases. The results are as follows:

24Ilm (in Fe-Ti oxide) + 8An (in Pl) + 8Qz + 18H_2O (in fluid) + O_2 (in fluid) = 4Ep + 4 Dph (in Chl) + 24Rt (1a)

Hem (in Fe-Ti oxide) + 5An (in Pl) + 2Qz + 3H_2O (in fluid) + 2K^+ (in fluid) = 2Ep + 2Ms + Ca^{2+} (in fluid) (1b)

Reaction (1a) requires the addition of O_2 (carried by fluid) to the reactants to produce Rt-C, indicating an oxidation process. Consequently, in addition to a pure element transfer, reaction (1a) involves a partial transformation of ferrous iron in the Fe-Ti oxides to ferric iron in epidote (Ep-C).

The product mineral assemblages demonstrate that the replacement reactions (1a) and (1b) occurred during greenschist-facies stage. Temperature conditions based on Zr-in-rutile thermometry indicate that the Rt-C in the veins crystallized at 476-515 °C (Fig. 7b). Rare thin coronas of rutile around Fe-Ti oxides, which are morphologically similar to the vein Rt-C, are also observed in the amphibolites (Fig. 2c), implying a similar replacement history and fluid infiltration process in both the metabasites and veins. However, a much higher Rt-C abundance is observed in the veins than in the amphibolites. This characteristic reflects that pre-existing vein systems may represent zones of structural weakness or rheological contrast (Spandler et al. 2011), which more readily allow the late-stage O_2-rich fluid influx.

Formation of Rt-S

Symplectitic intergrowths of Rt-S and magnetite after H-Ilm represent another type of replacement, which occurs only in the interior of the Fe-Ti oxides (Fig. 4a). The preservation of the size and external dimensions of the parent mineral and occurrence of relics of the reactant (H-Ilm) in the symplectites (Figs. 4b-4e) indicate that this replacement is associated only with the exsolved H-Ilm lamellae rather than

with whole Fe-Ti oxide grains. Although no hydrous minerals are observed in both the reactants and products, the following textural evidence implies that this type of replacement took place in the presence of a reactive fluid: (1) the Rt-Mag symplectite typically formed in regions near the brittle factures (Fig. 4a), and (2) various amounts and scales of micro voids or pores, which might have been previously fluid filled, are found in almost all of the symplectite domains (Figs. 4c and 4g), implying that the products are porous. All these features are consistent with a mineral re-equilibration process associated with fluid-involved dissolution-precipitation reactions (e.g., Putnis 2009; Spruzeniece et al. 2017). This interpretation is also in accordance with many previous studies (e.g., Viti et al. 2005), which showed that exsolution textures might provide good channels to allow fluid passage and mass transfer. The approximately pseudomorphic replacement implies that the dissolution and precipitation are spatially coupled under a low-strain condition (Putnis 2009; Putnis and John 2010).

Based on the mineral assemblages and compositions (Appendix Table 3) of the reactants (H-Ilm) and products (magnetite and rutile), we calculated the Rt-S-forming reaction by the THERMOCALC program. Magnetite activity was calculated using the method of White et al. (2002). The result is as follows:

$$6\text{Ilm (in H-Ilm)} + O_2\text{ (in fluid)} = 2\text{Mag} + 6\text{Rt} \qquad (2)$$

This reaction has been observed in both natural and experimental studies and is an important indicator of subsolidus oxidation processes (e.g., Lindsley 1991; Tan et al. 2015). Tan et al. (2015) stressed that oxidation led to the segregation of Fe^{3+} at the rutile-ilmenite interface and triggered the nucleation of magnetite along the margin of the growing Rt-S, which produced the distinctive vermicular morphology of the Rt-S.

Relationship of two types of replacements

The relationship between the two types of replacement reactions (formations of

the Rt-C and Rt-S) is difficult to define precisely because the detailed *P-T* conditions of the Rt-S cannot be directly constrained. However, the textural evidence clearly indicates that the reaction (2) occurred after the formation of H-Ilm lamellae (i.e., exsolution). Therefore, both two replacements occurred after the crystallization of the vein Fe-Ti oxides. We note that the Rt-S typically occurs in the Fe-Ti oxide grains that developed coronas of the Rt-C. In contrast, for the Fe-Ti oxide grains without Rt-C coronas, the replacement of H-Ilm by Rt-S is absent. These textural observations imply that both fluid-induced replacement reactions occurred in same stage and were controlled by a single fluid event. If this interpretation is correct, the Rt-S also formed during greenschist-facies stage (~476-515 °C) and Rt-C formed after the exsolution of H-Ilm from the Fe-Ti oxides.

Oxygen fugacity conditions during rutile-forming reactions

The reactions (1a) and (2) indicate the involvement of O_2 during the replacement of Fe-Ti phases by rutile. Therefore, oxygen fugacity conditions should have exerted an important impact on the stability of the rutile-bearing mineral assemblages. We calculated *T* versus f_{O_2} diagram for greenschist-facies conditions (with an assumed pressure of 0.5 GPa, Fig. 8) and estimated the f_{O_2} conditions of the reactions (1a) and (2) using the THERMOCALC program (Powell et al. 1998; version 3.33) with the thermodynamic database of Holland and Powell (2011). Four oxygen buffer reactions, i.e., magnetite-hematite (MH), Ni-NiO (NNO), fayalite-magnetite-quartz (FMQ), and iron-wüstite (IW), were plotted in the diagram for comparison (Fig. 8). Figure 8 shows that the curve of reaction (1a) intersects with the FMQ buffer at ~440 °C, whereas the curve of reaction (2) is parallel to the FMQ buffer, demonstrating that the f_{O_2} conditions for reaction (1a) are more dependent on temperature. Over the temperature range (476-515 °C) of Rt-C formation, reaction (1a) occurred under

oxidizing conditions, approximately 2.5-4.5 logf_{O_2} units above the FMQ buffer. These f_{O_2} values are very close to those of reaction (2) (~3.5 logf_{O_2} units above FMQ buffer for all temperatures). In particular, at ~500 °C (close to the average temperature of the Rt-C formation), the curves of the two reactions intersect, indicating identical f_{O_2} conditions for the two replacement reactions. These results further demonstrate that reactions (1a) and (2) most likely occurred during the same metamorphic stage and were controlled by a single fluid infiltrating event.

Braun and Raith (1985) applied ilmenite-magnetite oxygen barometry (Spencer and Lindsley 1981) to calculate f_{O_2} conditions for rutile growth during amphibolite- to greenschist-facies retrogression in metabasites from the eastern Alps. They obtained oxidizing conditions of ~5-6 logf_{O_2} above the FMQ buffer over a temperature range between 470 and 520 °C. Our present results, in combination with Braun and Raith (1985), indicate that retrograde LP rutile forms more readily under oxidizing conditions. We suggest that high f_{O_2} conditions are an important factor controlling the unusual replacement of Fe-Ti oxides by LP rutile in metabasites.

Origin of the infiltrating fluid

The hydrous mineral Ep-C, which coexists with the Rt-C, developed during the replacement process (Figs. 3f-3h). Therefore, the initial Sr isotopic compositions of the Ep-C provide information on the origin of the greenschist-facies infiltrating fluid. Based on reactions (1a) and (1b), the initial Sr isotopic values of the Ep-C should be controlled by two end members: the Sr-rich phase in the veins (plagioclase) and the high-f_{O_2} infiltrating fluid. As discussed earlier, the plagioclase veins formed from the internal dehydration of the host metabasites during amphibolitization. Therefore, the veins and vein plagioclase are expected to have same initial Sr isotopic composition as the metabasites.

The Ep-C has noticeably higher initial $^{87}Sr/^{86}Sr$ ratios than the metabasites (as well as the Ep-E and Ep-A) at the greenschist-facies stage (Fig. 6), indicating that the infiltrating fluid was not directly derived from the metabasites or plagioclase veins. Instead, this fluid must have originated externally from a source with significantly higher initial $^{87}Sr/^{86}Sr$ ratios. The occurrence of muscovite in replacement products indicates that the infiltrating fluid was derived from a K-rich source. The wall rocks of the metabasites, i.e., K-rich granitic gneisses, have much higher initial $^{87}Sr/^{86}Sr$ ratios than the metabasites at the greenschist-facies stage (Fig. 6). The initial $^{87}Sr/^{86}Sr$ ratios of the Ep-C vary between those of the metabasites (or Ep-E/Ep-A) and the gneisses. Therefore, we propose that the high-$^{87}Sr/^{86}Sr$ fluid was externally derived from the gneisses. This fluid buffered the low Sr isotopic values of the vein plagioclase and caused the product Ep-C to have initial Sr isotopic values ranging between those of the veins (metabasites) and the gneisses. This scenario is in accordance with many previous studies (e.g., Xiao et al. 2011; Guo et al. 2014, 2016; Li et al. 2016), which found that gneiss-derived retrograde fluids are typically relatively oxidizing. The large range of initial Sr isotopic values of the Ep-C reflects various degrees of interaction between the infiltrating fluid and the vein plagioclase.

Geochemical fingerprint of retrograde rutile and trace element behavior during replacement

Investigations of the HFSE and transition metal element (TME: Cr and V) contents of rutile and Fe-Ti oxides provide constraints on the chemical characteristics of the different types of rutile (Rt-E, Rt-A, and Rt-C) and element behavior during the replacement processes.

In the host metabasites, original rutile (Rt-E) was partially or totally replaced by polycrystalline Fe-Ti oxides during the amphibolite-facies stage, with or without relic

Rt-A cores (Figs. 2b-2d). The Rt-E and Rt-A have much higher contents of HFSEs (e.g., ~90 times for Nb) and lower contents of TMEs (e.g., 0.3-0.4 times for Cr) than the Fe-Ti oxides (Figs. 5a-5d), indicating that HFSEs were preferentially incorporated into rutile and that TMEs tended to enter Fe-Ti oxides during the replacement process, in accordance with the findings of many previous studies (e.g., Braun and Raith 1985; Luvizotto et al. 2009). Considering that consumption of each one gram of rutile could produce approximate five gram of Fe-Ti oxides (~21 wt.% TiO_2, Appendix Table 3), only a small proportion of HFSEs (<10 %) were redistributed into the Fe-Ti oxides during the replacement of rutile and the rest of HFSEs were excluded from the Fe-Ti oxide structure. On the contrary, the growth of Fe-Ti oxides at the expense of rutile requires the addition of external TMEs.

A small portion of the excluded HFSEs was likely redistributed into the relic rutile (Ep-A) via a back-diffusion process, which typically occurs when rutile is replaced by a mineral with a lower HFSE compatibility (e.g., titanite) (Lucassen et al. 2010; Cruz-Uribe et al. 2014). This prediction is supported by the fact that the Rt-A cores have a larger range of Nb contents and slightly higher contents of Nb and other HFSEs compared to the Rt-E (Figs. 5a-5c), which demonstrates that the original compositions of the Rt-E have been partially or completely obliterated. Thus, Rt-A is the relic Rt-E whose trace elements have been redistributed during amphibolite-facies metamorphism. The Nb/Ta ratios of the Rt-A are higher than those of the Rt-E (Fig. 5d), implying that more Nb than Ta propagated into the rutile via volume diffusion. This result is in consistent with the partitioning and diffusion of Nb and Ta in rutile (Klemme et al. 2005; John et al. 2011; Marschall et al. 2013). Nevertheless, Rt-A cores in the amphibolites are rarely preserved, which indicates that the released HFSEs should be also dominated by other mineral phases. Pargasite is a rock-forming

mineral (~45 vol%) in the amphibolites and in textural equilibrium with the Fe-Ti oxides. This mineral has been proven to be an important carrier of Nb and other HFSEs (e.g., Foley et al. 2002; Tiepolo and Vannucci 2014). Therefore, it is possible that the majority of the HFSEs released during the replacement of rutile during amphibolite-facies overprinting were distributed into pargasite.

In contrast, in the plagioclase veins, the Fe-Ti oxides were in turn replaced by polycrystalline rutile (Rt-C) at greenschist-facies stage. On the whole, Rt-C has trace element (especially Nb, Ta, and Cr) compositions and Nb/Ta ratios similar to those of the Fe-Ti oxides (Figs. 5a-5d), indicating that the chemical signatures of the Rt-C were mainly inherited from their precursor Fe-Ti oxides. The Fe-Ti oxides contain very small amounts of Nb and Ta and large amounts of Cr and V, making the product Rt-C to have noticeably low Nb (<10 ppm) and Ta (<2 ppm) contents, high Cr (>340 ppm) and V (>1580 ppm) contents, and low Nb/Ta ratios (<10) (Table 2; Figs. 5a-5d). These geochemical characteristics distinguish the Rt-C from the rutile formed during the high-grade metamorphism (Rt-E and Rt-A) in the host metabasites (high Nb-Ta contents and Nb/Ta ratios and low Cr-V contents) and provide a potential geochemical fingerprint for identifying the retrograde LP rutile. The large range of Nb contents in the Rt-C (Fig. 5a) is also in accordance with the observations of Luvizotto et al. (2009) and might be attributed to the continuous re-equilibrating process of the product rutile with the relic Fe-Ti oxides. Because the products of Rt-C-forming reactions include epidote, muscovite, and chlorite, which are also potential hosts of TMEs (Angiboust 2014; Guo et al. 2015), portions of the released Cr and V during this replacement process were likely also distributed into these three minerals as well as into the Rt-C.

IMPLICATIONS

Our results demonstrate that the Hualiangting amphibolite-vein system witnessed

multiple types of replacement and a complex fluid evolution history, which are related to variations in the physicochemical conditions during retrograde metamorphism of the UHP eclogites. Figure 9 summarizes the main processes involved in the formation of the Ti-rich phases following chronological order: (1) Rt-E grew during the UHP stage in the eclogite (Stage A, Fig. 9a); (2) Rt-E was replaced by the homogenous precursor (Ilm-Hem_{ss}) of the Fe-Ti oxides during amphibolitization (Stage B, Fig. 9b); (3) amphibolite-facies fluid flowed and dissolved Si, Al, Na, Ca, Fe, Ti, and other trace elements, which were then deposited in the plagioclase veins (Stages C, Figs. 9c and 9d); (4) subsolidus immiscibility in homogeneous Fe-Ti phases in both amphibolites and veins produced exsolved H-Ilm lamellae in the I-Hem matrix (Stage D, Figs. 9e and 9f); and (5) gneiss-derived high-fO_2 fluid infiltrated into the veins along grain boundaries between Fe-Ti oxides and plagioclase and/or between the exsolved H-Ilm lamellae and I-Hem matrix during greenschist-facies retrograde stage (Stage E, Fig. 9g), which led to the replacement of Fe-Ti oxides by polycrystalline Rt-C ± Ep-C ± MS ± Chl (reactions 1a and 1b, Fig. 9h) and the replacement of H-Ilm lamellae by symplectitic intergrowths of Rt-S + Mag (reaction 2, Fig. 9i). Similar replacement processes might also have occurred in the amphibolites (Fig. 9h).

Although most experimentally modelled phase relationships (e.g., Liou et al. 1998) and natural observations (Meinhold 2010 and references therein) have shown that, in subduction-zone metamorphic rocks, rutile generally forms under relatively high-grade (HT or HP-UHP) conditions, via the recrystallization of low-grade Fe-Ti oxides or Ti-rich silicates during prograde metamorphism, our new results highlight the fact that rutile can also grow during low-grade (greenschist-facies) retrograde overprinting of HP-UHP metabasites by fluid-driven replacement of Fe-Ti phases at relatively high-fO_2 conditions. These results, in line with a previous study (Braun and

Raith 1985), provide further constraints on the stability ranges of rutile and Fe-Ti oxides in metamorphic rocks. This finding is of particular petrological importance given that rutile can be used to determine the temperatures, ages, and geochemical evolution of these rocks. More care should be taken in the interpretation of rutile occurring in fluid-permeated polymetamorphic rocks because both high-grade and low-grade rutile phases may exist. Distinguishing the growth stages and metamorphic grades of rutile is the key to undertake its geological applications and subsequent interpretations.

Moreover, the present results, along with many previous investigations, indicate that episodic high-fO_2 fluid-induced oxidation events can occur in exhumed UHP slabs, such as during the stages of HP recrystallization (e.g., Mattinson et al. 2004; Cao et al. 2011; Li et al. 2016), amphibolite-facies retrogression (e.g., Guo et al. 2014, 2016), and greenschist-facies retrogression (Braun and Raith 1985 and this study). If these high-fO_2 fluids could be expelled from exhumed slabs and move upwards, they might cause an increase in the fO_2 condition and oxidation state of overlying mantle or crust rocks. Because Fe-Ti oxides are common phases in metabasites and HP-UHP rocks have generally experienced metasomatism during exhumation (e.g., Klemd 2013), the retrograde replacement of Fe-Ti oxides by LP rutile-bearing assemblages can be considered as a potential mineralogical indicator of oxidation in exhumed slabs. The distinctive geochemical features (low HFSE and high TME contents) can be used to identify this type of LP rutile in polymetamorphic subduction-zone rocks.

ACKNOWLEDGMENTS

This study was financially supported by The National Basic Research Program of China (973 Program, No. 2015CB856103) and The National Science Foundation of China (Nos. 41672059, 41372079, and 41525012). S.G. thanks the supports from the

Youth Innovation Promotion Association CAS (2017090). Constructive reviews from Drs. Alicia Cruz-Uribe and Emilie Janots significantly improved the manuscript. We also thank Dr. Thomas Mueller for his editorial handling. We thank Di Zhang, Yanbin Zhang, and Saihong Yang for the help during the EMP, LA(-MC)-ICP-MS, and BSE analyses.

REFERENCES CITED

Angiboust, S., Pettke, T., De Hoog, J.C.M., Caron, B., and Oncken, O. (2014) Channelized Fluid Flow and Eclogite-facies Metasomatism along the Subduction Shear Zone. Journal of Petrology, 55, 883-916.

Antignano, A., and Manning, C.E. (2008) Rutile solubility in H_2O, H_2O-SiO_2, and H_2O-$NaAlSi_3O_8$ fluids at 0.7–2.0 GPa and 700–1000 C: implications for mobility of nominally insoluble elements. Chemical Geology, 255, 283-293.

Austrheim, H., Putnis, C.V., Engvik, A.K., and Putnis, A. (2008) Zircon coronas around Fe–Ti oxides: a physical reference frame for metamorphic and metasomatic reactions. Contributions to Mineralogy and Petrology, 156, 517-527.

Ayers, J.C., Dunkle, S., Gao, S., and Miller, C.E. (2002) Constraints on timing of peak and retrograde metamorphism in the Dabie Shan ultrahigh-pressure metamorphic belt, east–central China, using U-Th-Pb dating of zircon and monazite. Chemical Geology 186, 315-331.

Bingen, B., Austrheim, H., and Whitehouse, M. (2001) Ilmenite as a source for zirconium during high-grade metamorphism? Textural evidence from the Caledonides of Western Norway and implications for zircon geochronology. Journal of Petrology, 42, 355-375.

Braun, E., and Raith, M. (1985) Fe-Ti-oxides in metamorphic basites from the eastern Alps, Austria: a contribution to the formation of solid solutions of natural Fe-Ti-oxide assemblages. Contributions to Mineralogy and Petrology, 90, 199-213.

Cao, Y., Song, S.G., Niu, Y.L., Jung, H., and Jin, Z.M. (2011) Variation of mineral composition, fabric and oxygen fugacity from massive to foliated eclogites during exhumation of subducted ocean crust in the North Qilian suture zone, NW China. Journal of Metamorphic Geology, 29, 699-720.

Chen, R.X., Zheng, Y.F., Gong, B., Zhao, Z.F., Gao, T.S., Chen, B., and Wu, Y.B. (2007) Origin of retrograde fluid in ultrahigh-pressure metamorphic rocks: constraints from mineral hydrogen isotope and water content changes in eclogite–gneiss transitions in the Sulu orogen. Geochimica et Cosmochimica Acta, 71, 2299-2325.

Connolly, J.A.D., and Cesare, B. (1993). C-O-H-S fluid composition and oxygen fugacity in graphitic metapelites. Journal of metamorphic geology, 11(3), 379-388.

Cruz-Uribe, A.M., Feineman, M.D., Zack, T., and Barth, M. (2014) Metamorphic reaction rates at ~650-800° C from diffusion of niobium in rutile. Geochimica et Cosmochimica Acta, 130, 63-77.

Ewing, T. A., Rubatto, D., Beltrando, M., and Hermann, J. (2015) Constraints on the thermal evolution of the Adriatic margin during Jurassic continental break-up: U–Pb dating of rutile from the Ivrea-Verbano Zone, Italy. Contributions to mineralogy and petrology, 169, 1-22.

Ewing, T. A., Rubatto, D., Eggins, S. M., and Hermann, J. (2011) In situ measurement of hafnium isotopes in rutile by LA–MC-ICPMS: protocol and applications. Chemical geology, 281, 72-82.

Ferry, J.M., and Watson, E.B. (2007) New thermodynamic models and revised calibrations for the Ti-in-zircon and Zr-in-rutile thermometers. Contributions to Mineralogy and Petrology, 154, 429-437.

Foley, S., Tiepolo, M., and Vannucci, R. (2002) Growth of early continental crust controlled by melting of amphibolite in subduction zones. Nature, 417, 837-840.

Gao, J., John, T., Klemd, R., and Xiong, X.M. (2007) Mobilization of Ti-Nb-Ta during subduction: Evidence from rutile-bearing dehydration segregations and veins hosted in eclogite, Tianshan, NW China. Geochimica et Cosmochimica Acta, 71, 4974-4996.

Guo, S., Chen, Y., Ye, K., Su, B., Yang, Y.H., Zhang, L.M., Liu, J.B., and Mao, Q. (2015) Formation of multiple high-pressure veins in ultrahigh-pressure eclogite (Hualiangting, Dabie terrane, China): Fluid source, element transfer, and closed-system metamorphic veining. Chemical Geology, 417, 238-260.

Guo, S., Yang, Y.H., Chen, Y., Su, B., Gao, Y. J., Zhang, L.M., Liu, J.B., and Mao, Q. (2016) Grain-scale Sr isotope heterogeneity in amphibolite (retrograded UHP eclogite, Dabie terrane): implications for the origin and flow behavior of retrograde fluids during slab exhumation. Lithos, 266-267, 383-405.

Guo, S., Ye, K., Chen, Y., Liu, J.B., Mao, Q., and Ma, Y.G. (2012) Fluid-rock interaction and element mobilization in UHP metabasalt: constraints from an omphacite-epidote vein and host eclogites in the Dabie orogen. Lithos, 136-139, 145-167.

Guo, S., Ye, K., Wu, T.F., Chen, Y., Zhang, L.M., Yang, Y.H., Liu, J.B., Mao, Q., and Ma, Y.G. (2013) A potential method to confirm the previous existence of lawsonite in eclogite: the mass imbalance of Sr and LREEs in multi-stage epidote (Ganghe, Dabie UHP terrane). Journal of Metamorphic Geology, 31, 415-435.

Guo, S., Ye, K., Yang, Y.H., Chen, Y., Zhang, L.M., Liu, J.B., Mao, Q., and Ma, Y.G. (2014) In situ Sr isotopic analyses of epidote: tracing the sources of multistage fluids in ultrahigh-pressure eclogite (Ganghe, Dabie terrane). Contributions to Mineralogy and Petrology, DOI: 10.1007/s00410-014-0975-9.

Harlov, D.E., Wirth, R., and Hetherington, C.J. (2011) Fluid-mediated partial alteration in monazite: the role of coupled dissolution–reprecipitation in element redistribution and mass transfer. Contributions to Mineralogy and Petrology, 162, 329-348.

Hébert, E., and Gauthier, M. (2007) Unconventional rutile deposits in the Quebec Appalachians: Product of hypogene enrichment during low-grade metamorphism. Economic Geology, 102, 319-326.

Hermann, J., Spandler, C., Hack, A., and Korsakov, A.V. (2006) Aqueous fluids and hydrous melts in high-pressure and ultra-high pressure rocks: implications for element transfer in

subduction zones. Lithos, 92, 399-417.

Holland, T.J.B., and Powell, R. (1998) An internally consistent thermodynamic data set for phase of petrological interest. Journal of Metamorphic Geology, 16, 309-343.

Holland, T.J.B., and Powell, R. (2011) An improved and extended internally consistent thermodynamic dataset for phases of petrological interest, involving a new equation of state for solids. Journal of Metamorphic Geology, 29, 333-383.

Janssen, A., Putnis, A., and Geisler, T. (2010) The experimental replacement of ilmenite by rutile in HCl solutions. Mineralogical Magazine, 74, 633-644.

John, T., Klemd, R., Klemme, S., Pfänder, J. A., Hoffmann, J. E., and Gao, J. (2011) Nb-Ta fractionation by partial melting at the titanite-rutile transition. Contributions to Mineralogy and Petrology, 161, 35-45.

Klemd, R. (2013) Metasomatism during high-pressure metamorphism: eclogites and blueschist-facies rocks. In D.E. Harlov and H. Austrheim, Ed., Metasomatism and the Chemical Transformation of Rock, p. 351-413. Springer Berlin Heidelberg.

Klemme, S., Prowatke, S., Hametner, K., and Günther, D. (2005) Partitioning of trace elements between rutile and silicate melts: implications for subduction zones. Geochimica et Cosmochimica Acta, 69, 2361-2371.

Li, D.Y., Xiao, Y.L., Li, W.Y., Zhu, X., Williams, H.M. and Li, Y.L. (2016) Iron isotopic systematics of UHP eclogites respond to oxidizing fluid during exhumation. Journal of Metamorphic Geology, 34, 987-997.

Li, Q.L, Li, S.G, Zheng, Y.F., Li, H.M, Massonne, H.J. and Wang, Q.C. (2003) A high precision U-Pb age of metamorphic rutile in coesite-bearing eclogite from the Dabie Mountains in central China: a new constraint on the cooling history. Chemical Geology, 200, 255-265.

Li, S.G, Jagoutz, E., Chen, Y., and Li, Q.L (2000) Sm–Nd and Rb–Sr isotopic chronology and cooling history of ultrahigh pressure metamorphic rocks and their country rocks at Shuanghe in the Dabie Mountains, Central China. Geochimica et Cosmochimica Acta, 64, 1077-1093.

Lindsley, D. H. (1973) Delimitation of the Haematite-Ilmenite Miscibility Gap. Geological Society of America Bulletin, 84, 657-662.

—— (1991) Experimental studies of oxide minerals. Reviews in Mineralogy and Geochemistry, 25(1), 69-106.

Liou, J.G., Zhang, R., Ernst, W.G., Liu, J., and McLimans, R. (1998) Mineral paragenesis in the Pianpaludo eclogitis body, Gruppo di Voltri, western Ligurian Alps. Schweizerische Mineralogische und Petrographische Mitteilungen 78, 317-335.

Liu, F.L., Gerdes, A., Zeng, L.S., and Xue, H.M. (2008) SHRIMP U–Pb dating, trace element and Lu–Hf isotope system of coesite-bearing zircon from amphibolite in SW Sulu UHP terrane, eastern China. Geochimica et Cosmochimica Acta, 72, 2973-3000.

Liu, F.L., and Liou, J.G. (2011) Zircon as the best mineral for P-T-time history of UHP metamorphism: A review on mineral inclusions and U-Pb SHRIMP ages of zircons from the

Dabie-Sulu UHP rocks. Journal of Asian Earth Sciences, 40, 1-39.

Lucassen, F., Dulski, P., Abart, R., Franz, G., Rhede, D., and Romer, R. L. (2010) Redistribution of HFSE elements during rutile replacement by titanite. Contributions to Mineralogy and Petrology, 160, 279-295.

Luvizotto, G.L., and Zack, T. (2009) Nb and Zr behavior in rutile during high-grade metamorphism and retrogression: an example from the Ivrea Verbano Zone. Chemical Geology 261, 303-317.

Luvizotto, G.L., Zack, T., Triebold, S., and von Eynatten, H. (2009) Rutile occurrence and trace element behavior in medium-grade metasedimentary rocks: example from the Erzgebirge, Germany. Mineralogy and Petrology, 97, 233–249.

Manning, C. E., Wilke, M., Schmidt, C., and Cauzid, J. (2008) Rutile solubility in albite-H_2O and $Na_2Si_2O_7$-H_2O at high temperatures and pressures by in-situ synchrotron radiation micro-XRF. Earth and Planetary Science Letters, 272, 730-737.

Marschall, H. R., Dohmen, R., and Ludwig, T. (2013) Diffusion-induced fractionation of niobium and tantalum during continental crust formation. Earth and Planetary Science Letters, 375, 361-371.

Massonne, H.J. (2012) Formation of amphibole and clinozoisite-epidote in eclogite owing to fluid infiltration during exhumation in a subduction channel. Journal of Petrology, 53, 1969-1998.

Mattinson, C.G., Zhang, R.Y., Tsujimori, T., and Liou, J.G. (2004) Epidote-rich talc-kyanite-phengite eclogites, Sulu terrane, eastern China: P-T-fO_2 estimates and the significance of the epidote-talc assemblage in eclogite. American Mineralogist, 89, 1772-1783.

Meinhold, G. (2010) Rutile and its applications in earth sciences. Earth-Science Reviews, 102, 1-28.

Meinhold, G., Anders, B., Kostopoulos, D., and Reischmann, T. (2008) Rutile chemistry and thermometry as provenance indicator: an example from Chios Island, Greece. Sedimentary Geology, 203, 98-111.

Mezger, K., Hanson, G.N., and Bohlen, S.R. (1989) High-precision U-Pb ages of metamorphic rutiles: application to the cooling history of high-grade terranes. Earth and Planetary Science Letters, 96, 106-118.

Miller, J.A., Buick, I.S., Cartwright, I., and Barnicoat, A. (2002) Fluid processes during the exhumation of high-P metamorphic belts. Mineralogical Magazine 12, 827-840.

Miller, J.A., and Cartwright, I. (2006) Albite vein formation during exhumation of high-pressure terranes: a case study from alpine Corsica. Journal of Metamorphic Geology, 24(5), 409-428.

Powell, R., Holland, T.J.B., and Worley, B. (1998) Calculating phase diagrams involving solid solutions via nonlinear equations, with examples using Thermocalc. Journal of Metamorphic Geology, 16, 577-588.

Putnis, A. (2009) Mineral replacement reactions. Reviews in mineralogy and geochemistry, 70, 87-124.

Putnis, A., and Austrheim, H. (2010) Fluid-induced processes: metasomatism and metamorphism. Geofluids, 10, 254-269.

Putnis, A., and John, T. (2010) Replacement processes in the Earth's crust. Elements, 6, 159-164.

Rapp, J.F., Klemme, S., Butler, I.B., and Harley, S.L. (2010) Extremely high solubility of rutile in chloride and fluoride-bearing metamorphic fluids: an experimental investigation. Geology, 38, 323-326.

Rečnik, A., Stanković, N., and Daneu, N. (2015) Topotaxial reactions during the genesis of oriented rutile/hematite intergrowths from Mwinilunga (Zambia). Contributions to Mineralogy and Petrology, 169, 1-22.

Rolfo, F., Compagnoni, R., Xu, S.T., and Jiang, L.L. (2000) First report of felsic whiteschist in the ultrahigh-pressure metamorphic belt of Dabie Shan, China. European Journal of Mineralogy 12, 883-898.

Rowe, M.C., Kent, A.J., and Nielsen, R.L. (2009) Subduction influence on oxygen fugacity and trace and volatile elements in basalts across the Cascade Volcanic Arc. Journal of Petrology, 50, 61-91.

Sakoma, E.M., and Martin, R.F. (2002) Oxidation-induced postmagmatic modifications of primary ilmenite, NYG-related aplite dyke, Tibchi complex, Kalato, Nigeria. Mineralogical Magazine, 66, 591-604.

Schmidt, A., Weyer, S., John, T., and Brey, G.P. (2009) HFSE systematics of rutile-bearing eclogites: New insights into subduction zone processes and implications for the earth's HFSE budget. Geochimica et Cosmochimica Acta, 73, 455-468.

Shi, Y.H., and Wang, Q.C. (2006) Variation in peak P-T conditions across the upper contact of the UHP terrane, Dabieshan, China: gradational or abrupt? Journal of Metamorphic Geology, 24, 803-822.

Spandler, C., Pettke, T., and Rubatto, D. (2011) Internal and external fluid sources for eclogite-facies veins in the Monviso meta-ophiolite, Western Alps: implications for fluid flow in subduction zones. Journal of Petrology, 52, 1207-1236.

Spear, F.S. (1993) Metamorphic phase equilibria and pressure-temperaturetime paths. Mineralogical Society of America Monograph, 799 p., Mineralogical Society of America, Washington, D.C.

Spencer, K.J., and Lindsley, D.H. (1981) A solution model for coexisting iron-titanium oxides. American mineralogist, 66, 1189-1201.

Spruzeniece, L., Piazolo, S., Daczko, N., Kilburn, M.R., and Putnis, A. (2017) Symplectite formation in the presence of a reactive fluid: Insights from hydrothermal experiments. Journal of Metamorphic Geology, DOI:10.1111/jmg.12231.

Strada, E., Talarico, F.M., and Florindo, F. (2006). Magnetic petrology of variably retrogressed eclogites and amphibolites: A case study from the Hercynian basement of northern Sardinia (Italy). Journal of Geophysical Research: Solid Earth, 111, B12S26,

doi:10.1029/2006JB004574.

Tiepolo, M., and Vannucci, R., (2014) The contribution of amphibole from deep arc crust to the silicate Earth's Nb budget. Lithos, 208, 16-20.

Tanis, E.A., Simon, A., Zhang, Y., Chow, P., Xiao, Y., Hanchar, J.M., Tschauner, O., and Shen, G. (2016) Rutile solubility in NaF-NaCl-KCl-bearing aqueous fluids at 0.5-2.79 GPa and 250-650 °C. Geochimica et Cosmochimica Acta, 177, 170-181.

Tan, W., Wang, C.Y., He, H., Xing, C., Liang, X., and Dong, H. (2015) Magnetite-rutile symplectite derived from ilmenite-hematite solid solution in the Xinjie Fe-Ti oxide-bearing, mafic-ultramafic layered intrusion (SW China). American Mineralogist, 100, 2348-2351.

Temple, A.K. (1966) Alteration of ilmenite. Economic Geology, 61, 695-714.

Tomkins, H.S., Powell, R. and Ellis, D.J. (2007) The pressure dependence of the zirconium-in rutile thermometer. Journal of Metamorphic Geology, 25, 703-713.

Viti, C., Mellini, M., and Rumori, C. (2005) Exsolution and hydration of pyroxenes from partially serpentinized harzburgites. Mineralogical Magazine, 69, 491-508.

Watson, E.B., Wark, D.A., and Thomas, J.B. (2006) Crystallization thermometers for zircon and rutile. Contributions to Mineralogy and Petrology, 151, 413-433.

White, R.W., Powell, R., and Clarke, G. L. (2002) The interpretation of reaction textures in Fe-rich metapelitic granulites of the Musgrave Block, central Australia: constraints from mineral equilibria calculations in the system K2O–FeO–MgO–Al2O3–SiO2–H2O–TiO2–Fe2O3. Journal of metamorphic Geology, 20, 41-55.

Whitney, D.L., and Evans, B. W. (2010) Abbreviations for names of rock-forming minerals. American Mineralogist, 95, 185-187.

Xiao, Y.L., Sun, W.D., Hoefs, J., Simon, K., Zhang, Z.M, Li, S. G., and Hofmann, A.W. (2006) Making continental crust through slab melting: constraints from niobium-tantalum fractionation in UHP metamorphic rutile. Geochimica et Cosmochimica Acta, 70, 4770-4782.

Xiao, Y.L., Hoefs, J., Hou, Z.H., Simon, K., and Zhang, Z.M. (2011) Fluid/rock interaction and mass transfer in continental subduction zones: constraints from trace elements and isotopes (Li, B, O, Sr, Nd, Pb) in UHP rocks from the Chinese Continental Scientific Drilling Program, Sulu, East China. Contributions to Mineralogy and Petrology, 162, 797-819.

Yang, T.N. (2004). Retrograded textures and associated mass transfer: evidence for aqueous fluid action during exhumation of the Qinglongshan eclogite, Southern Sulu ultrahigh pressure metamorphic terrane, eastern China. Journal of Metamorphic Geology, 22, 653-669.

Zack, T., Kronz, A., Foley, S. F., and Rivers, T. (2002) Trace element abundances in rutiles from eclogites and associated garnet mica schists. Chemical Geology, 184, 97-122.

Zack, T., Moraes, R., and Kronz, A. (2004) Temperature dependence of Zr in rutile: empirical calibration of a rutile thermometer. Contributions to Mineralogy and Petrology, 148, 471-488.

Zhang, R.Y., Liou, J.G., and Ernst, W.G. (2009) The Dabie-Sulu continental collision zone: A

comprehensive review. Gondwana Research, 16, 1-26.

Zhang, Z.M., Shen, K., Sun, W.D., Liu, Y.S., Liou, J.G., Shi, C., and Wang, J.L. (2008) Fluids in deeply subducted continental crust: petrology, mineral chemistry and fluid inclusion of UHP metamorphic veins from the Sulu orogen, eastern China. Geochimica et Cosmochimica Acta, 72, 3200-3228.

Zheng, Y.F., Zhao, Z.F., Wu, Y.B., Zhang, S.B., Liu, X., and Wu, F.Y. (2006) Zircon U-Pb age, Hf and O isotope constraints on protolith origin of ultrahigh-pressure eclogite and gneiss in the Dabie orogen. Chemical Geology, 231, 135-158.

Zheng, Y.F., Gao, X.Y., Chen, R. X., and Gao, T. (2011) Zr-in-rutile thermometry of eclogite in the Dabie orogen: Constraints on rutile growth during continental subduction-zone metamorphism. Journal of Asian Earth Sciences, 40, 427-451.

Figure captions

FIGURE 1. (a) Field view showing the vimineous plagioclase veins in the amphibolite (retrograded eclogite). **(b)** Polished hand-specimen of a vein (09HLT23V) enclosed in an amphibolite (09HLT23A). **(c)** Polished thin section showing Fe-Ti oxides in host amphibolites and plagioclase veins. Rutile corona (Rt-C) and silicate minerals (epidote and chlorite) are locally distributed around a Fe-Ti oxide crystal in the vein 09HLT23V. **(d)** and **(e)** Two photomicrographs showing the occurrence and texture of the Rt-C. Irregular Rt-C forming continuous coronas around the external edges of Fe-Ti oxides in the veins (09HLT23V and 09HLT24V). The Rt-C coexisting with muscovite and epidote (Ep-C).

FIGURE 2. Photomicrographs (**a, b, d**) and back-scattered electron (BSE) images (**c, e, f**) showing the rutile and Fe-Ti oxides in the eclogite 09HLT20 and amphibolite 09HLT23A. **(a)** Rutile in the UHP eclogite (Rt-E). **(b)** Partial or total replacement of rutile (Rt-A) by Fe-Ti oxides in the amphibolite. **(c)** A rutile grain partially replaced by polycrystalline Fe-Ti oxides in the amphibolite. Note that the Fe-Ti oxides are further surrounded by secondary Rt-C. **(d)** Fe-Ti oxides coexisting with plagioclase, epidote, and quartz in the amphibolite. **(e)** Internal textures of a Fe-Ti oxide mineral. **(f)** Exsolution of well-oriented hemo-ilmenite (H-Ilm) lamellae in the ilmeno-hematite (I-Hem) matrix. The coarse lamellae have widths of up to 4-8 μm, whereas the thin lamellae have widths of <1 μm. The mineral abbreviations are after Whitney and Evans (2010).

FIGURE 3. BSE images **(a, c, e-h)** and sketch maps **(b, d)** showing the replacement textures of Fe-Ti oxides by rutile-bearing assemblages in the veins. **(a)** and **(b)** Continuous coronas of polycrystalline Rt-C around the external edges of the Fe-Ti oxides. The boundary between the Fe-Ti oxides and Rt-C shows a zigzag shape

(09HLT23V). **(c)** and **(d)** Exsolution of a set of well-oriented H-Ilm lamellae from the I-Hem matrix in the Fe-Ti oxides. The coarse lamellae have widths of up to 10 μm, whereas the thin lamellae have widths of <1 μm (09HLT23V). **(e)** Several irregular Rt-C grains forming a discontinuous corona around the Fe-Ti oxides (09HLT23V). **(f)** Rt-C coexisting with Ep-C and chlorite (09HLT24V). **(g)** and **(h)** Rt-C coexisting with polycrystalline Ep-C fragments and muscovite (09HLT23V).

FIGURE 4. BSE images **(a, b, d)** and sketch map **(c, e)** showing the replacement textures of coarse H-Ilm lamellae by symplectites of rutile (Rt-S) and magnetite in the veins. **(a)** Symplectitic intergrowths of Rt-S + magnetite after coarse H-Ilm lamellae occurring near the fine fractures in Fe-Ti oxides (09HLT23V). **(b) and (c)** Replacement of coarse H-Ilm lamellae by vermicular-shaped Rt-S and interstitial magnetite. Note that H-Ilm relics occasionally occur in the symplectites. In addition, small amounts of voids or cavities are observed in the symplectites (09HLT23V). **(f)** and **(g)** Variously sized (up to several tens of μm) intergranular voids or cavities are common in the symplectites or along the boundaries between the symplectites and Fe-Ti phases (09HLT24V).

FIGURE 5. Plots of Cr *vs.* Nb **(a)**, Cr *vs.* Zr **(b)**, V *vs.* Nb **(c)**, and Cr *vs.* Nb/Ta **(d)** showing the compositional characteristics of multiple types of rutile and Fe-Ti oxides.

FIGURE 6. Plots of X_{Fe} *vs.* initial $^{87}Sr/^{86}Sr$ ratios showing the composition and Sr isotopic compositions of various types of epidote (t = 230 Ma for Ep-E; t = 210 Ma for Ep-A; and t = 200 Ma for Ep-C) in the metabasites and veins. The whole-rock initial Sr isotopic data (t = 200 Ma) of amphibolites, eclogites, and gneisses (Guo et al. 2015, 2016) are also plotted for comparison.

FIGURE 7. Frequency histograms showing calculated formation temperatures of

Rt-E **(a)** and Rt-C in the veins **(b)** using Zr-in-rutile thermometer of Tomkins et al. (2007). Pressures used for calculations are 3.5 GPa (Rt-E) and 0.5 GPa (Rt-C). Inset in **(b)** indicates that the Rt-C in the veins coexists with zircon and quartz.

FIGURE 8. Log fO_2-T diagram calculated by the THERMOCALC program (Powell et al. 1998; version 3.33) and the thermodynamic database of Holland and Powell (2011) at 0.5 GPa showing the oxygen fugacity conditions of replacement reactions (1a) and (2). Activities of plagioclase, ilmenite, hematite, epidote, and chlorite were calculated from measured compositions by the AX program of Holland and Powell (1998). Magnetite activity was calculated using the method of White et al. (2002). Quartz, water, and rutile were treated as pure end-member phases. Four oxygen reference buffers – MH (magnetite-hematite), NNO (Ni-NiO), FMQ (fayalite-magnetite-quartz), and IW (iron-wüstite) – are plotted for comparison. The blue rectangle represents the temperature range of the Rt-C formation, which was constrained by the Zr-in-rutile thermometer. The curve of reaction (1a) intersects with the FMQ buffer at ~440 °C, while the curve of reaction (2) is parallel to the FMQ buffer. The curve of reaction (1a) intersects with that of reaction (2) at ~500 °C.

FIGURE 9. Schematic sketch (not to scale) showing the formation of retrograde LP rutile (Rt-C and Rt-S) in the metabasite-vein system. **(a)** Rutile (Rt-E) was stable during UHP metamorphism. **(b)** During amphibolite-facies retrogression, Rt-E was partially or totally replaced by Fe-Ti oxides, with or without relic rutile (Rt-A). Along with amphibolitization, amphibolite-facies fluids flowed, migrated, and dissolved Si, Al, Na, Ca, Fe, Ti and other components in the amphibolites. **(c)** and **(d)** Plagioclase veins crystallized from the fluids, and Fe-Ti oxides precipitated in the veins. At this stage, the Fe-Ti oxides (Ilm-Hem_{ss} precursors) had homogenous compositions. **(e)** and **(f)** With further cooling, temperatures decreased to that of the miscibility gap of

Ilm-Hem_{ss}, and the H-Ilm lamellae exsolved from the I-Hem matrix. **(g)** High-f_{O_2} fluid from the gneisses infiltrated into the veins and metabasites along the grain boundaries between plagioclase and Fe-Ti oxides and/or between the H-Ilm lamellae and I-Hem matrix during greenschist-facies stage. **(h)** Fluid infiltration led to the replacement of Fe-Ti oxides by polycrystalline Rt-C ± Ep ± Ms ± Chl via reaction (1a). **(i)** Fluid infiltration led to the replacement of H-Ilm lamellae by symplectitic intergrowths of Rt-S + magnetite via reaction (2). **(j)** P-T evolution of Hualiangting metabasites and veins (modified from Guo et al. 2015).

This is a preprint, the final version is subject to change, of the American Mineralogist (MSA)
Cite as Authors (Year) Title. American Mineralogist, in press.
(DOI will not work until issue is live.) DOI: http://dx.doi.org/10.2138/am-2017-6120

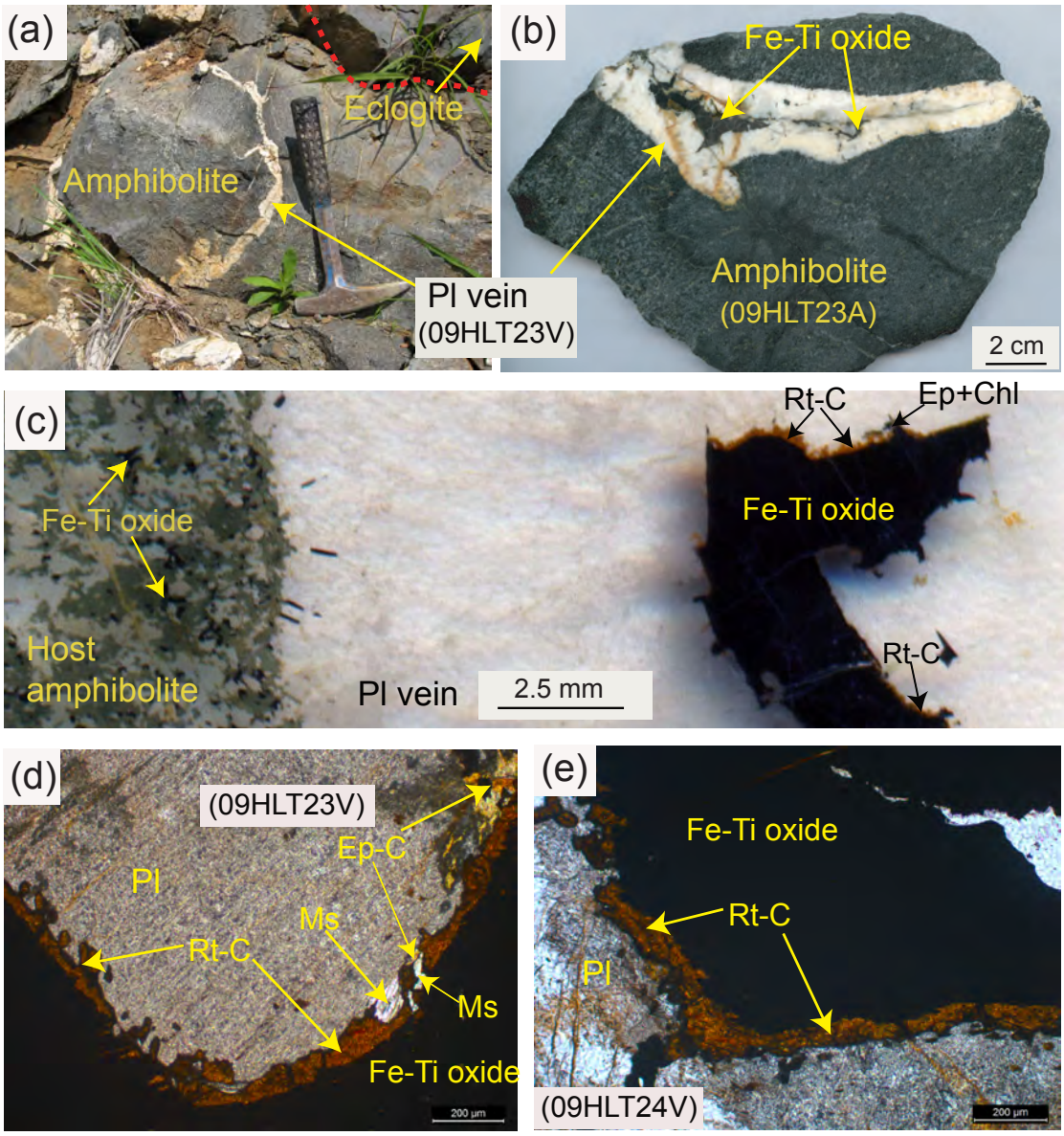

Fig. 1

This is a preprint, the final version is subject to change, of the American Mineralogist (MSA)
Cite as Authors (Year) Title. American Mineralogist, in press.
(DOI will not work until issue is live.) DOI: http://dx.doi.org/10.2138/am-2017-6120

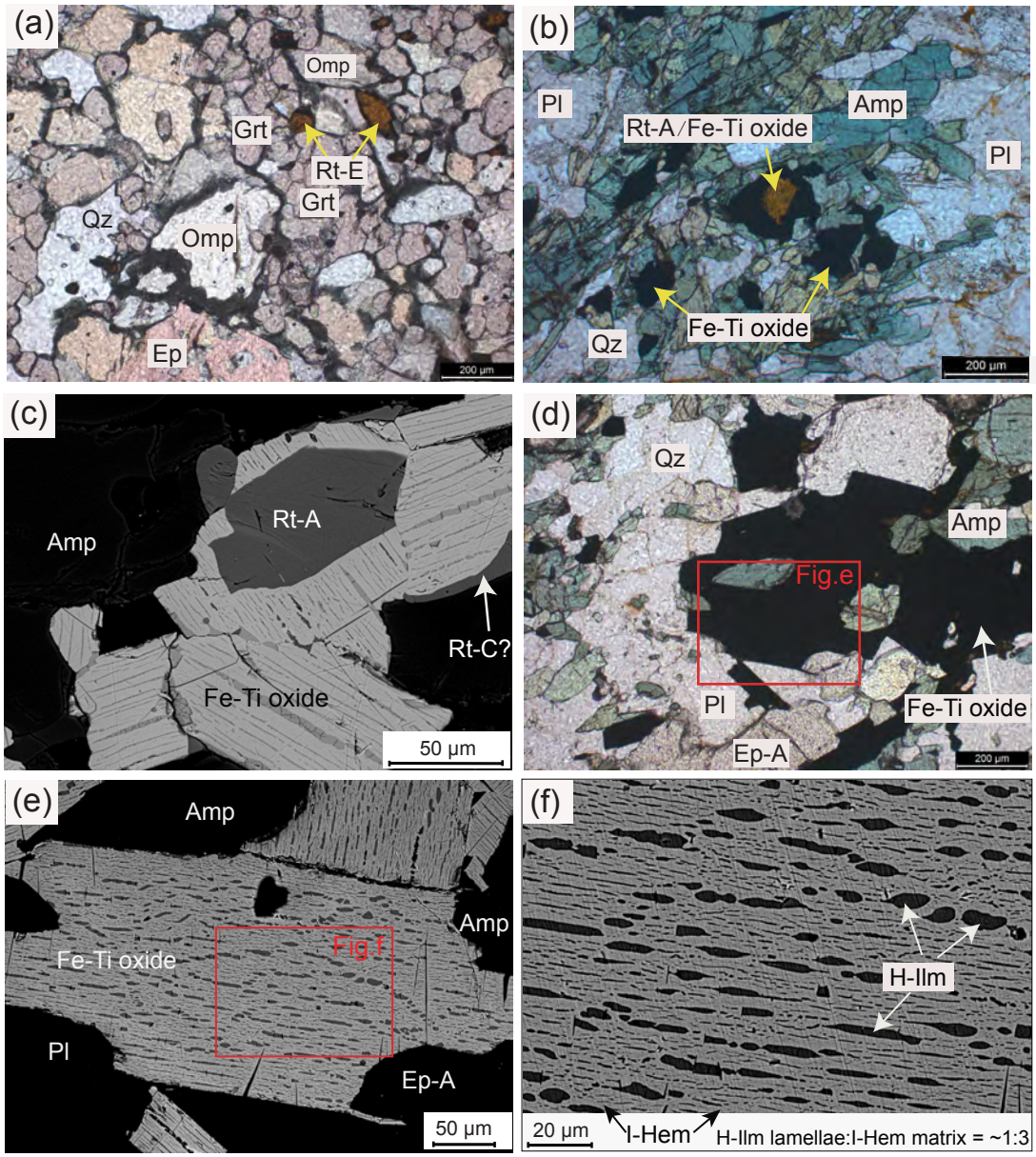

Fig. 2

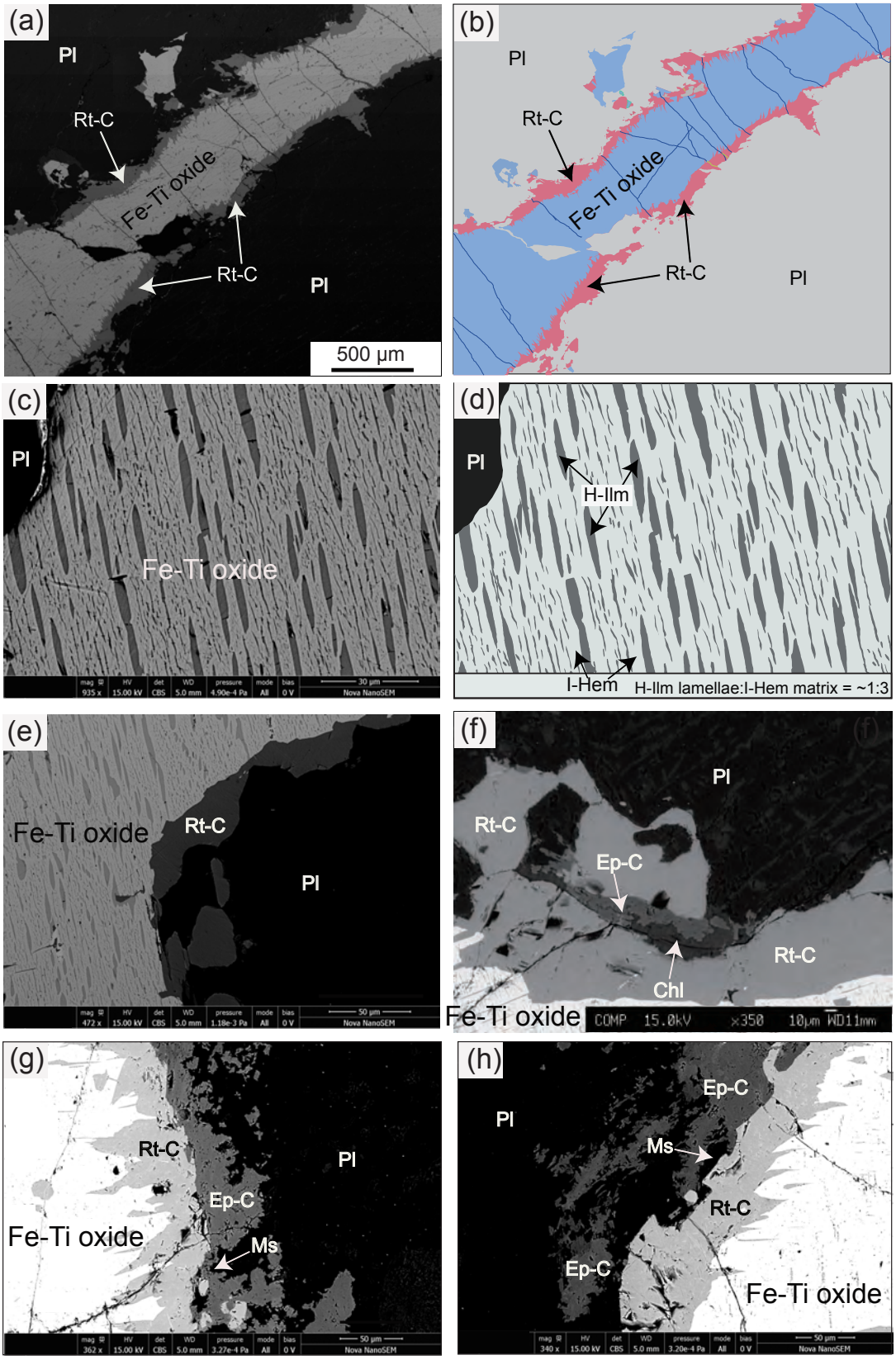
(a)
Pl
Rt-C
Fe-Ti oxide
Rt-C
Pl
500 µm
(b)
Pl
Rt-C
Fe-Ti oxide
Rt-C
Pl
(c)
Pl
Fe-Ti oxide
(d)
Pl
H-Ilm
I-Hem
H-Ilm lamellae:I-Hem matrix = ~1:3
(e)
Fe-Ti oxide
Rt-C
Pl
(f)
Pl
Rt-C
Ep-C
Rt-C
Chl
Fe-Ti oxide
COMP 15.0kV ×350 10µm WD11mm
(g)
Rt-C
Pl
Ep-C
Fe-Ti oxide
Ms
(h)
Ep-C
Pl
Ms
Rt-C
Ep-C
Fe-Ti oxide

Fig. 3

This is a preprint, the final version is subject to change, of the American Mineralogist (MSA)
Cite as Authors (Year) Title. American Mineralogist, in press.
(DOI will not work until issue is live.) DOI: http://dx.doi.org/10.2138/am-2017-6120

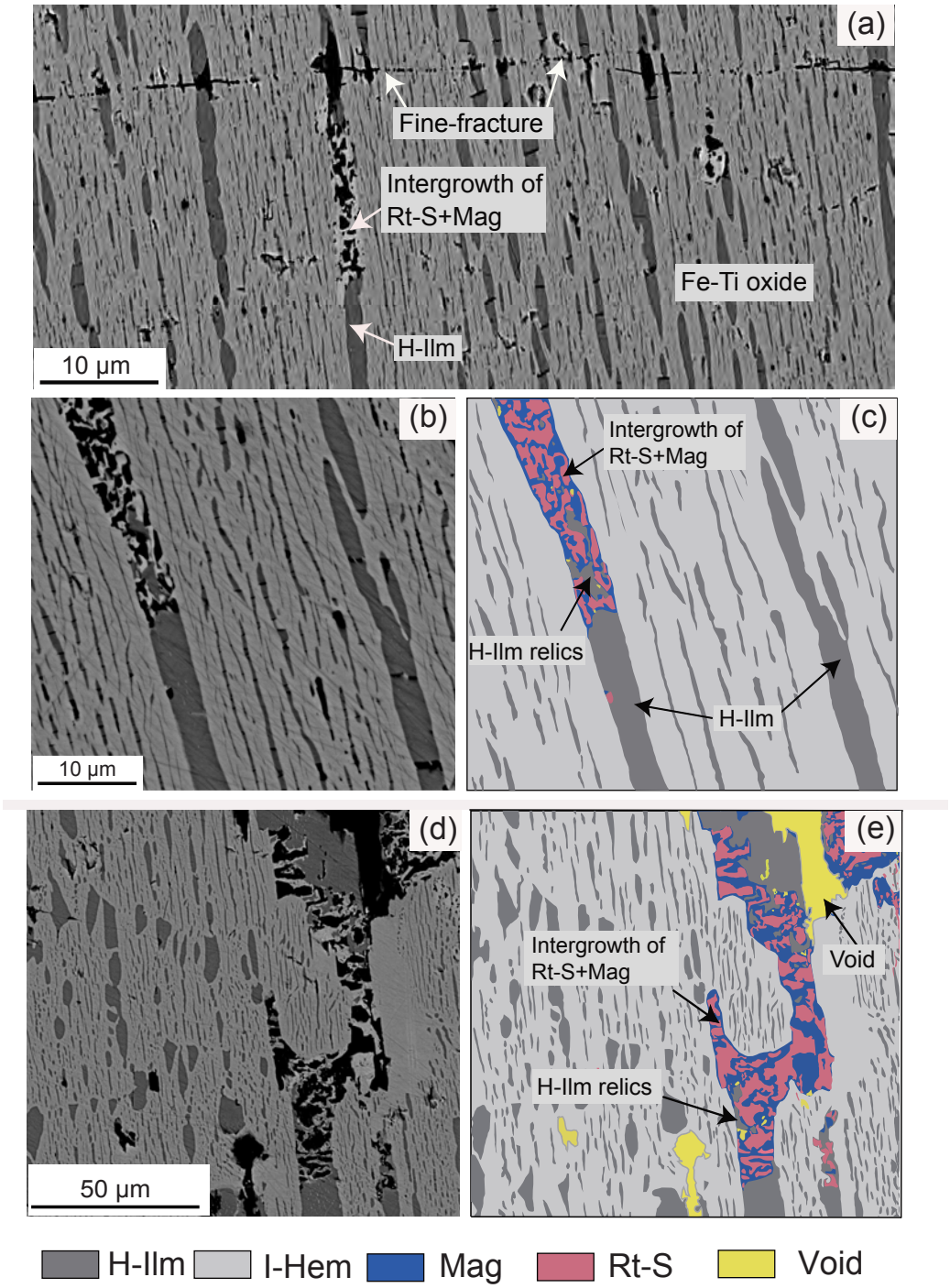

Fig. 4

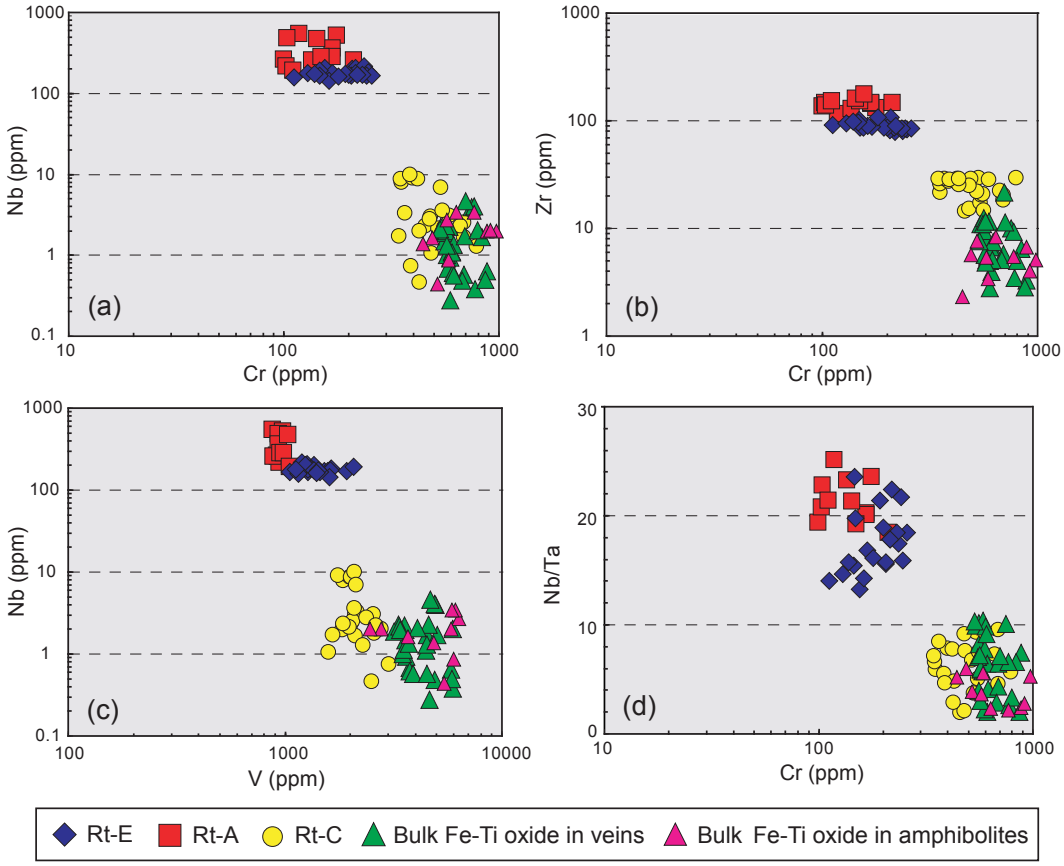
(a)
Nb (ppm)
Cr (ppm)
(b)
Zr (ppm)
Cr (ppm)
(c)
Nb (ppm)
V (ppm)
(d)
Nb/Ta
Cr (ppm)
Rt-E
Rt-A
Rt-C
Bulk Fe-Ti oxide in veins
Bulk Fe-Ti oxide in amphibolites

Fig. 5

This is a preprint, the final version is subject to change, of the American Mineralogist (MSA)
Cite as Authors (Year) Title. American Mineralogist, in press.
(DOI will not work until issue is live.) DOI: http://dx.doi.org/10.2138/am-2017-6120

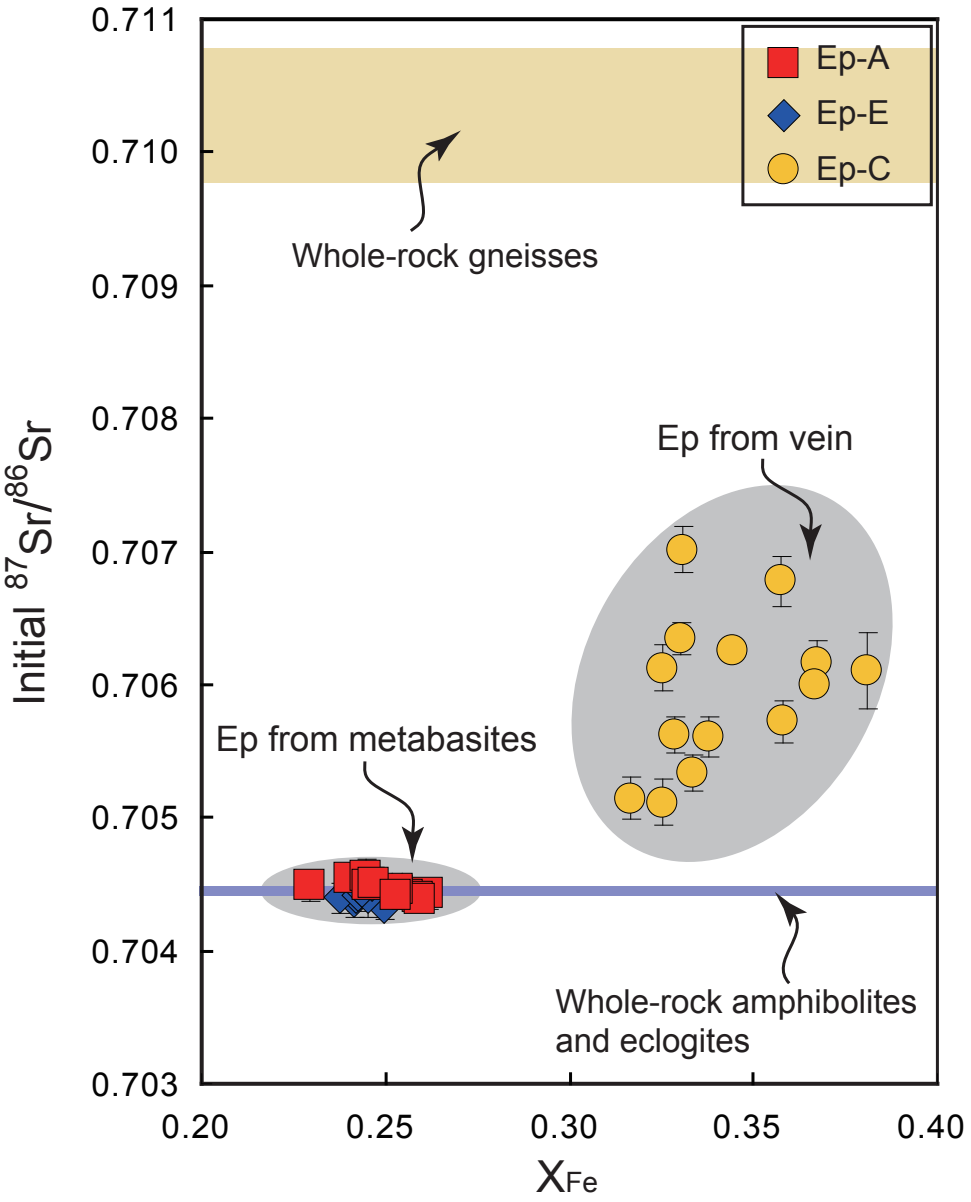

Fig. 6

This is a preprint, the final version is subject to change, of the American Mineralogist (MSA)
Cite as Authors (Year) Title. American Mineralogist, in press.
(DOI will not work until issue is live.) DOI: http://dx.doi.org/10.2138/am-2017-6120

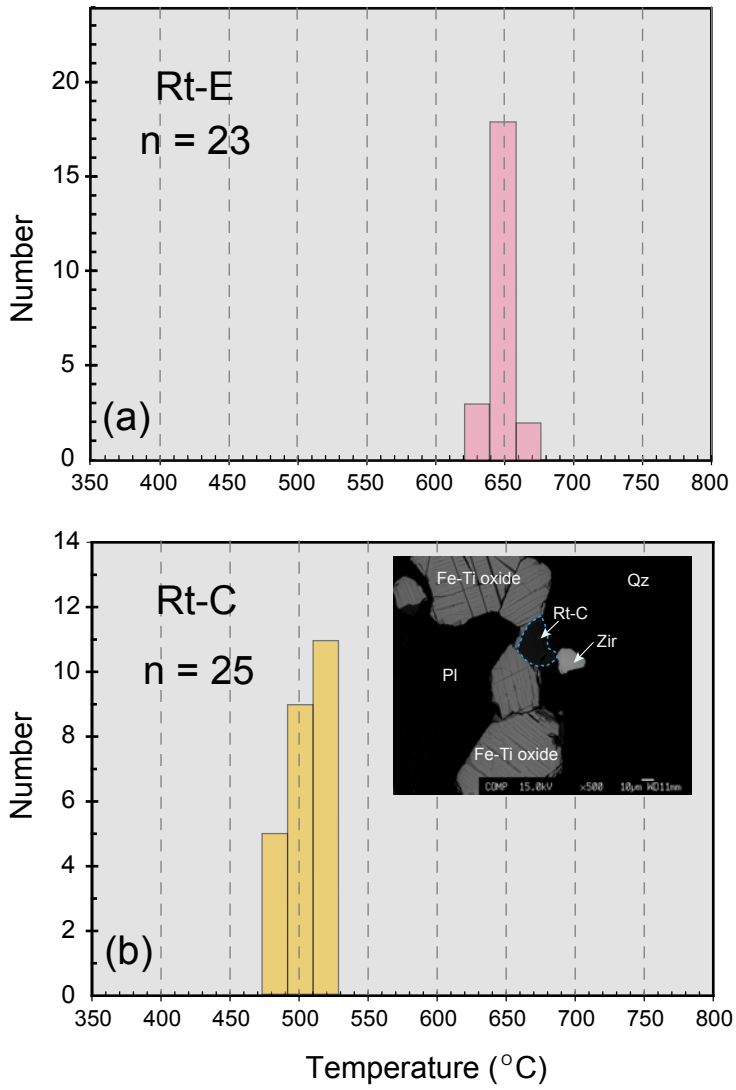

Fig. 7

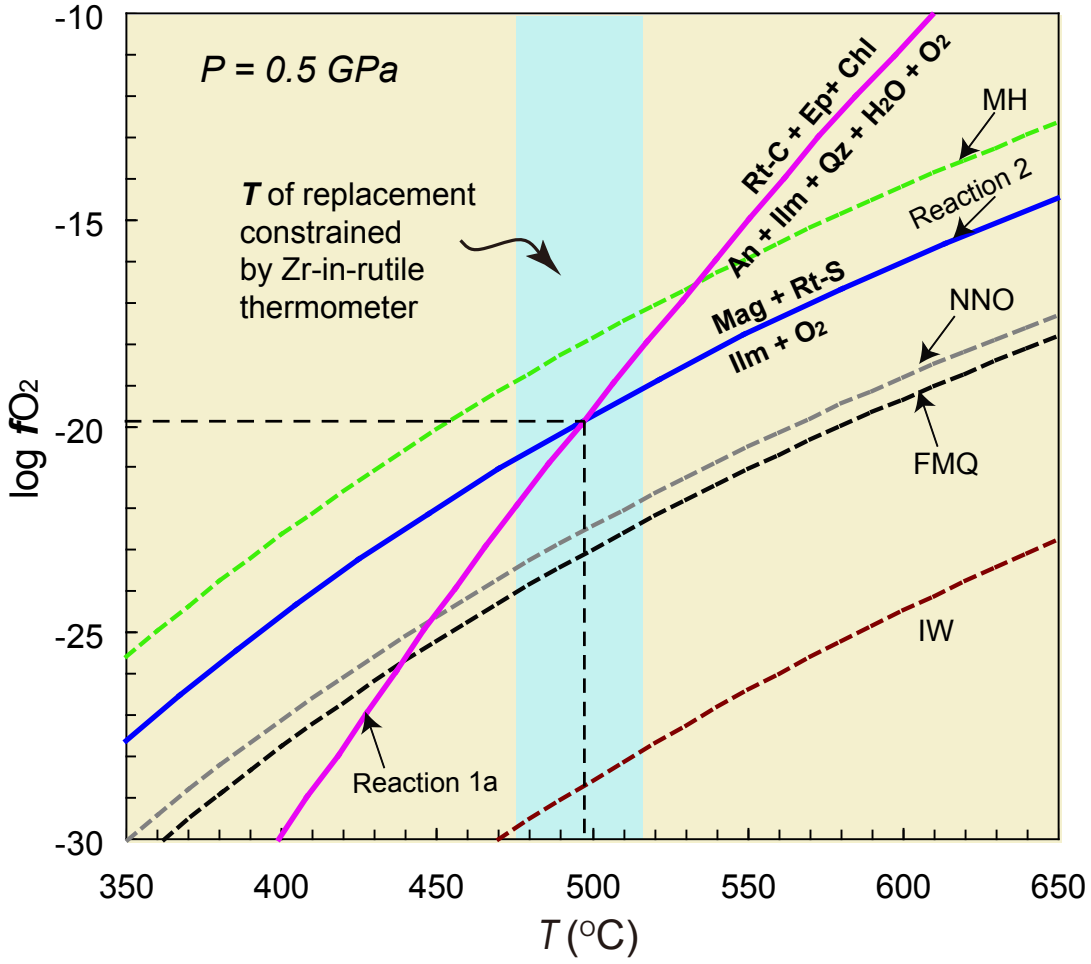
P = 0.5 GPa
T of replacement constrained by Zr-in-rutile thermometer
Rt-C + Ep+ Chl
An + Ilm + Qz + H2O + O2
MH
Reaction 2
Mag + Rt-S
Ilm + O2
NNO
FMQ
IW
Reaction 1a
log fO2
T (°C)
-10
-15
-20
-25
-30
350
400
450
500
550
600
650

Fig. 8

This is a preprint, the final version is subject to change, of the American Mineralogist (MSA)
Cite as Authors (Year) Title. American Mineralogist, in press.
(DOI will not work until issue is live.) DOI: http://dx.doi.org/10.2138/am-2017-6120

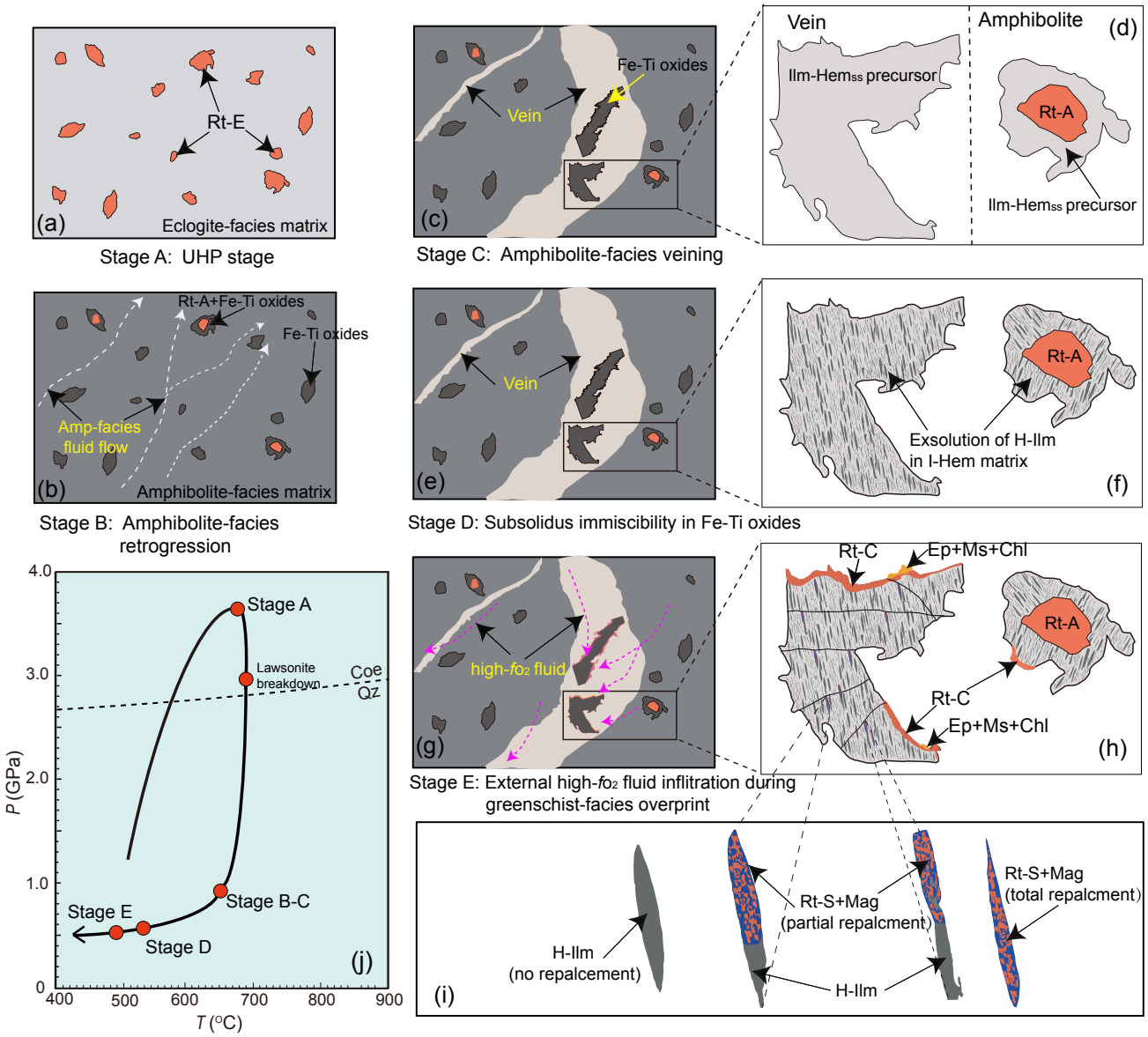

Fig. 9

Table 1 Main characteristics of each type of rutile in the metabasite-vein system, defined by texture, coexisting mineral, metamorphic stage, temperature condition, mineral chemistry, and formation mechanism

Rutile types	Rt-E	Rt-A	Rt-C	Rt-S
Host rock	Eclogite	Amphibolite	Plagioclase vein	Plagioclase vein
Sample	09HLT20, 09HLT21	09HLT23A, 09HLT24A	09HLT23V, 09HLT24V	09HLT23V, 09HLT24V
Occurrence and texture	Anhedral, accessory mineral	Relic cores in Fe-Ti oxides	Small, rounded to flat, polycrystalline coronas around the external edges of Fe-Ti oxides	fine-grained vermicular symplectite after exsolved H-Ilm
Coexisting mineral	Omp, Grt, coe, Ep-E, Ap, and Zir	—	Ep-C, Ms, Chl, Qz, Ap, and Zir	Mag
Metamorphic stage	UHP eclogite-facies	Amphibolite-facies	Greenschist-facies	Greenschist-facies
Zr-in-rutile thermometry	636-659 °C	—	476-515 °C	Close to the Rt-C
Trace element chemistry	High Nb (140-210 ppm), Ta (8-12 ppm), Zr (79-108 ppm), Hf (2-6 ppm), Cr (110-260 ppm) and V (1050-2080 ppm); high Nb/Ta ratios (13-24)	Very high Nb (190-540 ppm), Ta (9-22 ppm), Zr (117-175), and Hf (3-5); low Cr 100-180 ppm) and V (880-1050 ppm); very high Nb/Ta ratios (16-25)	Low Nb (0.5-10 ppm), Ta (0.1-1.8 ppm), Zr (15-30 ppm), Hf (0.4-6 ppm); high Cr (340-790 ppm) and V (1580-3010 ppm); low Nb/Ta ratios (2-10)	Not analyzed
Formation mechanism	Primary UHP phase	Relic eclogite-facies rutile whose trace elements have been redistributed during amphibolite-facies retrogression	Replacement product of Fe-Ti oxides	Replacement product of H-Ilm lamellae

Table 2 Trace element compositions of various types of rutile (ppm) and calculated temperatures

Minerals	Nb	Ta	Zr	Hf	Cr	V	Sn	Nb/Ta	Zr/Hf	Temperature (°C)
Rt-E in eclogite 09HLT20										
	203	12.0	108	3.65	207	1360	21.6	16.9	29.6	659
	205	10.5	79	2.16	216	1261	23.7	19.5	36.6	636
	215	11.4	80	4.46	236	1194	28.3	18.9	17.9	637
	167	10.6	82	3.05	206	1277	22.2	15.8	26.9	639
	184	11.6	84	2.36	246	1312	17.7	15.9	35.6	640
	165	7.6	84	2.35	242	1411	21.3	21.7	35.7	640
	166	9.0	85	2.01	257	1054	13.8	18.4	42.3	641
	172	9.3	85	2.38	233	1513	16.4	18.5	35.7	641
	177	9.9	86	2.16	215	1270	21.2	17.9	39.8	642
	182	9.2	86	4.76	149	1628	16.3	19.8	18.1	642
	169	8.9	86	2.91	200	1574	23.5	19.0	29.6	642
	176	8.2	86	2.58	193	1614	18.8	21.5	33.3	642
Rt-E in eclogite 09HLT21										
	204	15.4	87	3.58	155	1245	16.4	13.2	24.3	643
	176	10.5	89	5.87	169	1357	18.2	16.8	15.2	644
	171	7.6	89	6.11	219	1933	16.8	22.5	14.6	644
	144	10.1	89	2.47	162	1601	18.3	14.3	36.0	644
	191	8.1	101	2.17	147	2077	17.1	23.6	46.5	654
	157	10.2	91	2.21	112	1151	19.8	15.4	41.2	646
	177	11.1	95	4.32	129	1123	25.8	15.9	22.0	649
	165	10.7	97	3.01	146	1450	25.6	15.4	32.2	651
	175	10.1	99	2.5	138	1422	21.6	17.3	39.6	652
	163	9.1	107	2.51	180	1397	19.3	17.9	42.6	658
	185	8.8	102	2	153	1986	17.1	21.0	51.0	655
Rt-A in amphibolite 09HLT23A										
	541	21.5	117	2.84	118	878	13.5	25.2	41.2	—
	255	11.0	129	3.53	136	923	15.0	23.2	36.5	—
	280	14.0	146	3.39	168	948	11.5	20.0	43.1	—
	265	13.7	135	4.58	100	920	12.4	19.3	29.5	—
	218	10.5	147	3.61	103	943	14.0	20.8	40.7	—

488	21.4	139	3.53	104	931	13.4	22.8	39.4	—
359	17.7	143	3.45	168	931	13.7	20.3	41.4	—
257	14.0	145	3.02	211	885	11.6	18.4	48.0	—
Rt-A in amphibolite 09HLT24A									
284	14.8	153	2.99	150	984	12.5	19.2	51.2	—
524	22.2	131	4.07	177	980	13.1	23.6	32.2	—
192	9.0	153	3.98	111	1049	13.9	21.3	38.4	—
469	22.0	162	4.25	143	1032	13.0	21.3	38.1	—
278	17.5	175	3.42	156	980	11.6	15.9	51.2	—
Rt-C in vein 09HLT23V									
2.28	1.16	14.5	1.25	456	2010	11.8	2.0	11.6	476
3.02	1.43	15.2	1.37	480	2112	11.9	2.1	11.1	479
2.77	0.303	25.0	1.07	478	2373	5.10	9.1	23.4	506
8.67	1.31	26.0	1.98	350	2005	13.5	6.6	13.1	508
9.01	1.16	28.0	1.75	399	1758	12.5	7.8	16.0	512
8.69	1.12	28.7	5.71	422	2012	15.3	7.8	5.0	514
9.91	1.80	27.5	4.26	385	2094	13.7	5.5	6.5	511
1.96	0.526	29.2	1.35	528	1839	7.11	3.7	21.6	515
3.29	0.390	29.1	1.75	366	2152	8.52	8.4	16.6	515
2.52	0.550	20.4	1.13	689	2048	10.5	4.6	18.1	495
3.06	0.434	28.5	0.95	589	2558	12.4	7.1	30.0	513
1.70	0.240	28.9	1.62	344	1655	5.47	7.1	17.8	514
1.05	0.139	29.0	1.39	485	1584	9.29	7.6	20.9	514
Rt-C in vein 09HLT24V									
6.88	1.000	17.4	1.08	538	2130	8.49	6.9	16.1	486
1.68	0.176	18.2	1.26	689	2107	7.15	9.5	14.4	488
3.60	0.386	20.6	1.56	545	2088	11.0	9.3	13.2	495
1.79	0.356	20.7	1.36	555	2586	5.94	5.0	15.2	495
2.13	0.315	21.9	1.27	521	1986	4.14	6.8	17.2	498
2.32	0.317	22.2	1.12	665	1862	7.41	7.3	19.8	499
7.88	1.34	21.5	1.52	351	1851	12.5	5.9	14.1	497
2.01	0.418	25.2	1.30	428	2767	3.38	4.8	19.4	506
0.741	0.158	28.4	1.18	389	3010	3.23	4.7	24.1	513
0.461	0.159	28.7	1.20	428	2509	4.74	2.9	23.9	514

1.28	0.226	29.3	1.29	789	2284	5.47	5.7	22.7	515
2.20	0.294	14.6	0.39	557	2627	7.28	7.5	37.4	477

The temperatures were calculated using the Zr-in-rutile thermometer of Tomkins et al. (2007).
Pressures used for Rt-E and Rt-C calculations were 3.5 GPa and 0.5 GPa, respectively.